



Design, synthesis and biological evaluation of novel indolinedione–coumarin hybrids as xanthine oxidase inhibitors

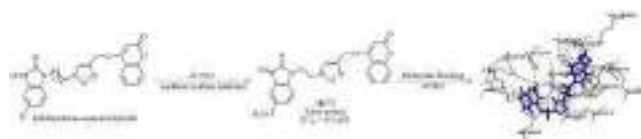
Harmandeep Kaur Gulati¹ · Kavita Bhagat¹ · Atamjit Singh¹ · Nitish Kumar¹ · Arshmeet Kaur¹ · Akriti Sharma¹ · Shilpa Heer¹ · Harbinder Singh¹ · Jatinder Vir Singh¹ · Preet Mohinder S. Bedi¹

Received: 21 January 2020 / Accepted: 8 June 2020
© Springer Science+Business Media, LLC, part of Springer Nature 2020

Abstract

A library of indolinedione–coumarin hybrid molecules was rationally designed and synthesized against hyperuricemia. All of the synthesized hybrid molecules were tested to check their inhibitory activity against xanthine oxidase enzyme by using a spectrophotometric assay. The results revealed that the compound showed IC_{50} values within the range of 6.5–24.5 μ M amongst which compound **K-7** was found to be endowed with the most potent IC_{50} value against xanthine oxidase enzyme. Kinetic studies were also performed to check the mode of inhibition of most potent compound **K-7**, which revealed its mixed-type inhibition behavior. Structure-activity relationships revealed that electron-donating groups and small alkyl chains between the two active scaffolds might be beneficial in inhibiting xanthine oxidase enzyme. It was also shown that various electrostatic interactions stabilized the compound **K-7** within the active site of xanthine oxidase enzyme, which confirmed that it can completely block its catalytic active site. Thus, **K-7** is regarded as a potent xanthine oxidase inhibitor and can be served as a promising molecular architectural unit for anti-hyperuricemic drug design.

Graphical Abstract



Keywords Indolinedione · Coumarin · Hybrids · Xanthine oxidase enzyme · Enzyme kinetics · Molecular docking studies

Introduction

Xanthine oxidase (XO), a molybdoflavoprotein containing iron and molybdenum, that promotes the oxidation, especially of hypoxanthine to xanthine and then to uric acid (UA) with the release of hydrogen peroxide and superoxide anions during the process of purines catabolism in humans. A well-known relationship exists between XO and hyperuricemia, a condition which is characterized by elevated serum UA level (7 mg/dL) (Wortmann 1998). Impairment in purine metabolism results in the deposition of sodium urate crystals in joints, which further causes inflammation and pain in joints. With this aspect, XO acts as an important and selective target for sustaining broad-spectrum chemotherapy in hyperuricemic patients (Ojha et al. 2017; Kumar et al. 2011).

Supplementary information The online version of this article (<https://doi.org/10.1007/s00044-020-02589-2>) contains supplementary material, which is available to authorized users.

- ✉ Harbinder Singh
singh.harbinder40@gmail.com
- ✉ Jatinder Vir Singh
jatindervirsingh1@gmail.com
- ✉ Preet Mohinder S. Bedi
bedi_preet@yahoo.com

¹ Department of Pharmaceutical Sciences, Guru Nanak Dev University, Amritsar, Punjab 143005, India

In the recent past, numerous successful purine based XO inhibitors such as allopurinol, pterin and 6-formylpterin (Oetl and Reibneggar 1999), 2-alkylhypoxanthines (Oetl and Reibneggar 1999; Biagi et al. 2001; Brien et al. 1985), and 2-substituted 7Hpyrazolo-[4,3-e]-1,2,4-triazolo-[1,5-c]-pyrimidines (Nagamatsu et al. 2000; Nagamatsu et al. 1985; Nagamatsu et al. 1995; Ali et al. 2010) are used for the treatment of hyperuricemia. These derivatives were mainly associated with the number of side effects (Stevens–Johnson syndrome and drug rash with eosinophilia and systematic symptoms (Ali et al. 2010; Pacher et al. 2006; Hille 2006) and also hindered the activities of both purine and pyrimidine metabolizing enzymes, which motivate the researchers around the globe to develop non-purine XO inhibitors (Pacher et al. 2006; Hille 2006; Borges et al. 2002).

Therefore, researchers paid great attention to the development of non-purine XO inhibitors. The compound BOF-4272, a potent XO inhibitor, its clinical use was limited because variation occurring in its efficacy which is mainly due to the difference in hepatic metabolism (Pacher et al. 2006). Febuxostat, a non-purine XO inhibitor that was approved from European Medicines Evaluation Agency and USFDA showed efficient efficacy with improved hypouricemic effect as compared with Allopurinol (Osada et al. 1993; Komoriya et al. 1993; Becker et al. 2004). Besides this, it was also reported that Febuxostat showed some side effects similar to Allopurinol such as headache, diarrhea, dizziness, abnormalities in liver function, and nausea (Strilchuk et al. 2019; Love et al. 2010; Becker et al. 2007; Schumacher et al. 2008; Becker et al. 2007). Furthermore, pyranostat was found to show higher in vivo efficacy with a poor pharmacokinetic profile (Ishibuchi et al. 2001; Sebastian et al. 2016). Whereas, topiroxostat, another non-purine based XO inhibitor, was also showed significant activity but with similar side effects as allopurinol (Pascart and Richette 2018). Based on these particular results, it can be concluded that researchers that involved in this field must develop alternate scaffolds that act as potent XO inhibitors with lesser side effects that can be used for the treatment of hyperuricemia.

Besides these, many researchers have also focussed on XO inhibitors derived from natural compounds-flavonoids, hydroxycinnamic acids, tannins, chalcones, saponins, terpenoids, stilbenes, phenylethanoid glycosides, since these can act as lead compounds for the discovery of new synthetics (Malik et al. 2018; Mehmood et al. 2019).

Coumarin is a natural moiety that is known to its various biological activities, also found to be a potent XO inhibitor. Numerous reports on the XO inhibitory potential of coumarin derivatives are available (Fais et al. 2018; Chen et al. 2014). Figure 1 depicts recently reported coumarin derivatives with XO inhibitory potential. Therefore, it could be an

ideal moiety to be included in the novel alternative molecular architecture for the further development of XO inhibitors.

From the last 5 years, we are continuously working on the similar lines to develop non-purine based XO inhibitors (Dhiman et al. 2012; Shukla et al. 2014; Sharma et al. 2014; Virdi et al. 2014; Kaur et al. 2015; Kaur et al. 2015, Kaur et al. 2017; Singh et al. 2019; Kaur et al. 2019) and now, we have come up with a new series of coumarin hybrid molecules clubbed with indolinedione with the help of triazole moiety as a linker. The rationale for the inclusion of indolinedione to the designed molecules is very clear. The two carbonyl groups and the nitrogen atom of the indole ring could act as hydrogen bond acceptor in the active site of the XO enzyme, which was confirmed through molecular modeling studies in the current evaluation. 1,2,3-triazole is also an active moiety owing to its three H-bond acceptor-Nitrogen atoms, the inclusion of which could also be beneficial for its better interactions within the XO enzyme.

Results and discussion

Indolinedione–coumarin hybrids were synthesized by following the synthetic Scheme 1. At first, substituted indolinediones were stirred with 1,2-dibromoalkanes (1 eq) at room temperature using Dimethylformamide (DMF) as a solvent, and potassium carbonate (1.5 eq) as a base. The resulting product was then dissolved in DMF and then sodium azide (1 eq) was added. The reaction mixture was stirred at room temperature to form 1-(4-azidoalkyl)indoline-2,3-diones.

Then, 4-hydroxycoumarin and propargyl bromide (1.2 eq) were stirred in DMF under basic conditions (K_2CO_3 ; 1.5 eq) to obtain 4(prop-2-ynyloxy)-2H-chromen-2-one (PHC).

This 4-(prop-2-ynyloxy)-2H-chromen-2-one (PHC) was further reacted with various 1-(4-azidoalkyl)indoline-2,3-dione analogues in the presence of pentahydrate $CuSO_4$ (catalytic amount) and sodium ascorbate (as a reducing agent of $CuSO_4$), in DMF at room temperature to obtain the desired hybrid compounds. All compounds were monitored by thin-layer chromatography in the reaction, purified by column chromatography. 1H NMR and ^{13}C NMR spectroscopic techniques were used to characterize the synthesized compounds and all the spectral data was found in accordance with assumed structures.

In vitro xanthine oxidase assay

All the synthesized compounds were evaluated to test their inhibition against XO enzyme at five different concentrations ranging from 1 to 50 μM . The formation of UA was determined by using UV spectrophotometer at 292 nm and

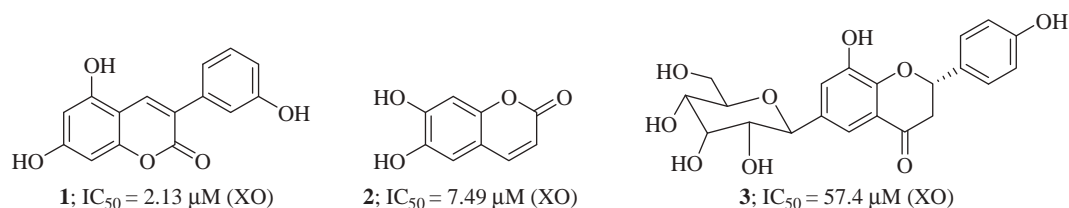
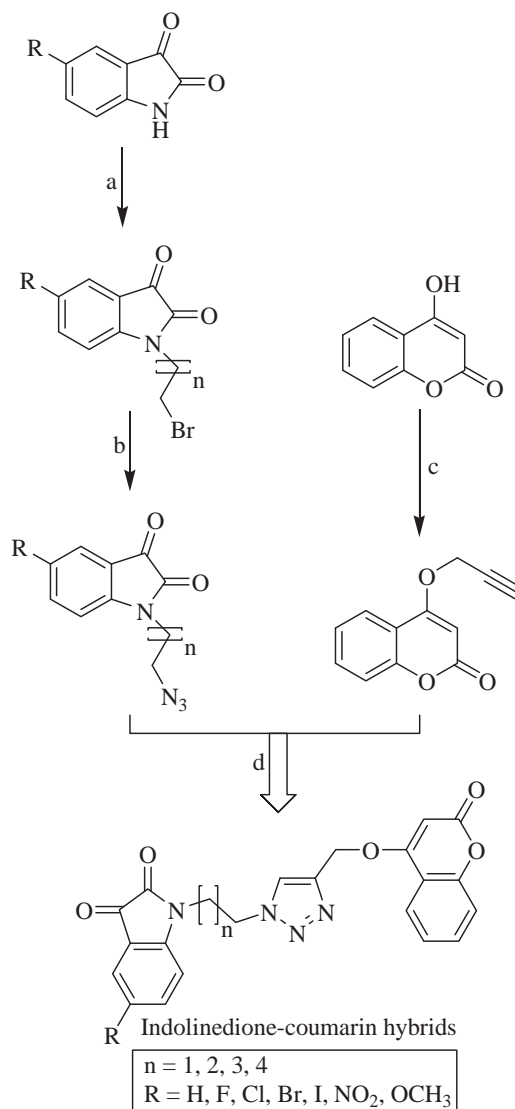


Fig. 1 Recently reported potent coumarin derivatives as XO inhibitors

Scheme 1 Synthesis of indolinedione-coumarin hybrids. Reagents and conditions: (a) dibromoalkanes, K_2CO_3 , DMF, 2 h, stir, rt; (b) NaN_3 , DMF, 1 hr, stir, rt; (c) Propargyl bromide, K_2CO_3 , DMF, 2 h, stir, rt; (d) Sodium ascorbate, $CuSO_4$, DMF, 15 min, rt



Code	n	R
K-1	1	H
K-2	1	F
K-3	1	Cl
K-4	1	Br
K-5	1	I
K-6	1	NO_2
K-7	1	OCH_3

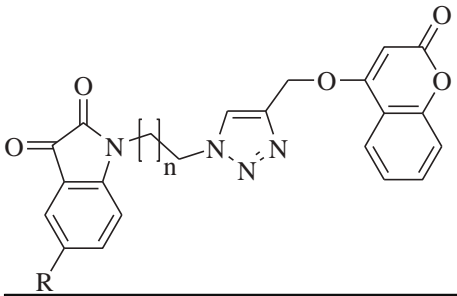
Code	n	R
L-1	2	H
L-2	2	F
L-3	2	Cl
L-4	2	Br
L-5	2	I
L-6	2	NO_2
L-7	2	OCH_3

Code	n	R
M-1	3	H
M-2	3	F
M-3	3	Cl
M-4	3	Br
M-5	3	I
M-6	3	NO_2
M-7	3	OCH_3

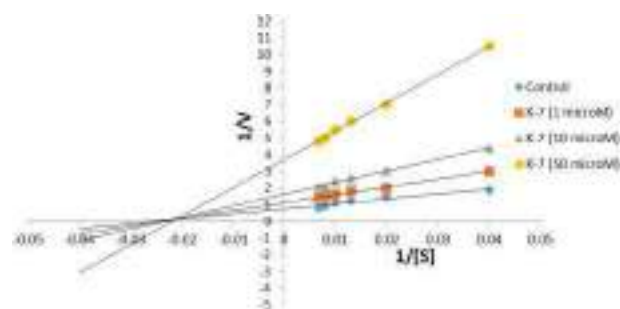
percentage inhibition was calculated for each compound. (Table 1). The results of the assay revealed that compounds showed good to moderate inhibition. Two compounds (**K-1** & **K-7**) showed above 80% inhibition against the enzyme at $50 \mu M$ concentration, while some displayed below 30% inhibition even at $50 \mu M$ concentration. The concentration at which 50% of the enzyme was inhibited, was calculated only for those compounds which inhibited the enzyme

above 50% at $50 \mu M$ concentration. Two compounds (**K-1** & **K-7**) were found to be endowed with the most prominent inhibition with the IC_{50} values of $8.9 \mu M$ and $6.5 \mu M$, respectively. The IC_{50} values of all the compounds were ranging from 6.5 to $24.5 \mu M$. The results revealed that the structural architecture of the compounds greatly influences the inhibitory activity. For instance, the compounds bearing electron-donating groups ($-OCH_3$) on 5th position of

Table 1 Xanthine oxidase inhibitory activity of all the synthesized compounds

								
Compound	R	n	Percent inhibition					IC ₅₀ (μM)
			1 (μM)	5 (μM)	10 (μM)	25 (μM)	50 (μM)	
K-1	H	1	32	42	62	79	85	8.9 ± 0.12
K-2	F	1	20	29	39	52	57	18.4 ± 1.9
K-3	Cl	1	24	30	40	56	61	15.6 ± 1.43
K-4	Br	1	23	34	45	60	65	14.3 ± 1.23
K-5	I	1	23	39	48	59	70	11.4 ± 1.08
K-6	NO ₂	1	21	30	38	53	59	12.5 ± 1.09
K-7	OCH ₃	1	35	49	69	85	92	6.5 ± 0.09
L-1	H	2	25	29	41	57	63	15.7 ± 1.45
L-2	F	2	12	19	25	34	45	–
L-3	Cl	2	11	17	28	39	49	–
L-4	Br	2	19	28	34	51	57	24.5 ± 2.87
L-5	I	2	21	30	40	53	60	17.8 ± 1.98
L-6	NO ₂	2	10	17	26	32	44	–
L-7	OCH ₃	2	23	40	49	60	69	12.4 ± 0.98
M-1	H	3	9	15	21	30	44	–
M-2	F	3	3	5	9	18	30	–
M-3	Cl	3	4	8	13	22	38	–
M-4	Br	3	8	14	20	27	39	–
M-5	I	3	7	13	21	28	41	–
M-6	NO ₂	3	2	8	17	24	29	–
M-7	OCH ₃	3	19	30	37	51	55	20 ± 1.76
Allopurinol								8.16 ± 1.27

indolinedione moiety enhanced the activity as compared with the compounds bearing electron-withdrawing groups (halogen atoms). The chain length between indolinedione and triazole moieties also affects the activity, as the chain length increases the inhibitory activity gradually decreases. Therefore, the activity order for substitution on 5th position of indolinedione followed as: $-\text{OCH}_3 > \text{H} > \text{I} > \text{Br} > \text{Cl} > \text{F} \approx \text{NO}_2$ and for chain length (n): $1 > 2 > 3$. From these results, it has been cleared that relatively compounds with high molecular weight are less potent than that of small molecules. This can be explained on the basis of the size of the active pocket of the enzyme XO, which is relatively very small and those compounds which can well occupy in the cavity showed the inhibitory activity (Table 1). This was also confirmed through molecular modeling studies in section (Molecular modelling studies).

**Fig. 2** Lineweaver–Burk plot of **K-7**

Enzyme kinetics

Compound **K-7** was further investigated for the type of inhibition by performing enzyme kinetic studies (Fig. 2). The pattern of the Lineweaver–Burk plot graph shows that

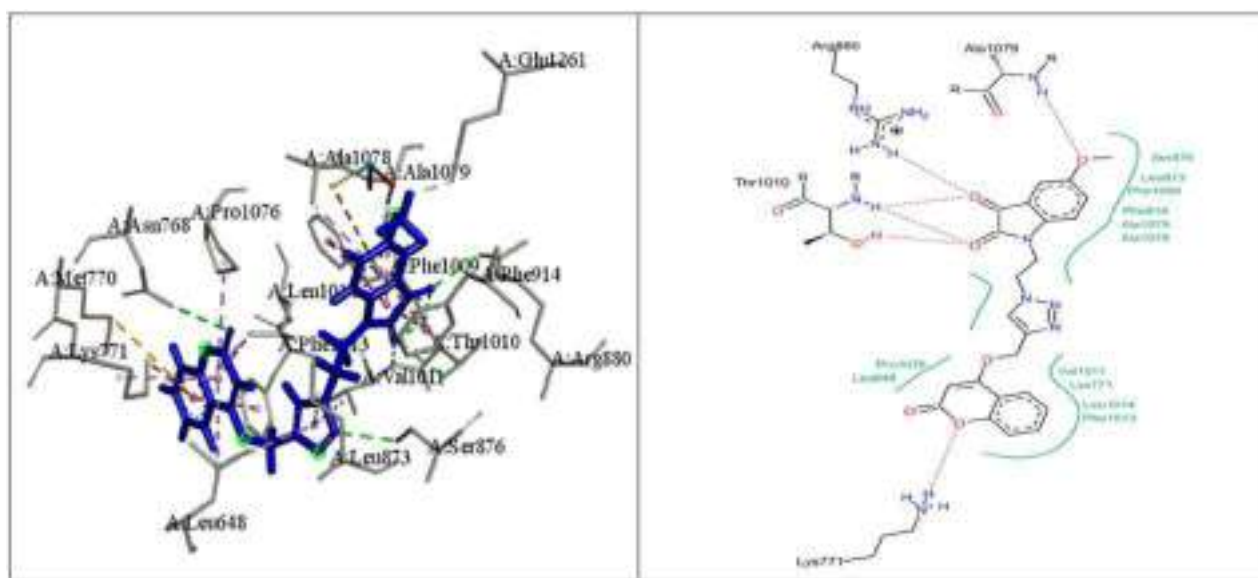


Fig. 3 3D representation of **K-7** (blue) within the active site of XO enzyme (Left-hand side), 2D representation of **K-7** within the active site of the enzyme (right-hand side)

it is a form of mixed inhibition scenario where K_m , V_{max} , and slope are all affected by the inhibitor. The inhibitor has increased the K_m and slope (K_m/V_{max}) while decreasing the V_{max} . Moreover, on careful observation, it was found that intersecting lines on the graph converge to the left of the y-axis and above the x-axis which indicates that the value of α (a constant that defines the degree to which inhibitor binding affects the affinity of the enzyme for substrate) is >1 (Copeland 2005). This confirms that the inhibitor preferentially binds to the free enzyme and not the enzyme-substrate complex. Therefore, the mode of inhibition of **K-7** is mixed-type but it seems that it has a strong competitive component.

Molecular modeling studies

Molecular modeling studies were performed to elucidate interactions of the most potent compound **K-7** within the active site of XO enzyme. The X-ray crystallographic structure of XO, complexed with febuxostat (PDB entry: 1N5X; resolution 2.8 Å) was employed. The accuracy of the docking program was validated by docking co-crystallized ligand febuxostat in its binding pocket. The program was able to reproduce best fit confirmation of febuxostat with a root mean square deviation of 0.523 indicating the reliability of docking protocol. After that, compound **K-7** was docked into febuxostat binding site and its top best pose with dock score of -32.2563 was selected for discussion (Fig. 3).

Overall binding mode of compound **K-7** with residues of the binding site suggests that compound fits well in the

cavity and is well stabilized by various electrostatic interactions. Major interactions with XO enzyme include π -sigma, π -alkyl, carbon-hydrogen bond, π -donor hydrogen bond, and conventional hydrogen bond interaction. Indolinedione moiety is well positioned in a cavity formed by hydrophobic residues Ser876, Leu873, Phe1009, Phe914, Ala1079, and Ala1078. The methoxy group present on the 5th position of indolinedione forms the conventional hydrogen bond with the amine group of Ala1079. Three additional hydrogen bonds are formed as expected with the two carbonyl groups of indolinedione with amino acid residues Arg880 and Thr1010. On the other end, coumarin moiety is inserted into the cavity formed by various hydrophobic amino acids Pro1076, Leu648, Val1011, Lys771, Leu1014, and Phe1013 and also stabilized by H-bond interaction with Lys771 through an oxygen atom of pyran ring (Fig. 3). Therefore, docking studies suggest that the **K-7** completely blocks the binding pocket of the XO enzyme to exert its inhibitory action which also supports its potent in vitro activity.

Conclusion

Coumarin and indolinedione are multifunctional products and in the current study, we have rationally designed and synthesized various Indolinedione–coumarin molecular hybrids. Their bioactivities were evaluated in terms of their XO inhibitory potential. Almost all of the compounds were found active while two compounds **K-1** and **K-7** showed better results in vitro and were potent ones as compared

with standard drug allopurinol. Structure-activity relationship revealed that the compounds with electron-donating groups ($-\text{OCH}_3$) increased the activity and length of two carbon chain between indolinedione and triazole moieties are most favorable, one for the inhibitory potential. Kinetic studies indicated that **K-7** showed its mixed-type inhibition scenario against the XO enzyme. Various binding interactions of **K-7** with the active site of the XO enzyme were also streamlined by using docking studies. Therefore, these compounds could act as hit lead molecules for the further development of potent XO inhibitors.

Experimental

Material and measurements

The chemical reagents were procured from CDH, Sigma-Aldrich, and Loba, India. All yields refer to isolated products after purification. Products were characterized by comparing with authentic samples and by spectroscopic techniques i.e., ^1H and ^{13}C NMR, Elemental Analysis). Avance III HD 500 MHz Bruker Biospin and JEOL AL 300 MHz machines were used to record the NMR spectra. The spectra were recorded by dissolving in CDCl_3 and $\text{DMSO}-d_6$ relative to TMS (0.00 ppm). In ^1H NMR chemical shifts were reported in δ values using an internal standard (tetramethylsilane) with a number of protons, multiplicities (s-singlet, d-doublet, t-triplet, q-quartet, m-multiplet) and coupling constants (J) in Hertz (Hz). Melting points were determined in open capillaries and were uncorrected.

General procedure for the synthesis of 4-(prop-2-ynyloxy)-2H-chromen-2-one (PGC)

In 50 mL of DMF, 4-Hydroxy coumarin (20 g) was dissolved with the addition of propargyl bromide (1.2 eq) and K_2CO_3 (1.5 eq). The reaction mixture was stirred at room temperature and the reaction was continuously monitored by TLC. After the completion of the reaction, the reaction mixture was poured on crushed ice. The solid product of propargylated coumarin thus obtained was filtered, washed with cold water, and air-dried. The physical data of propargylated coumarin is given below:

4-(prop-2-ynyloxy)-2H-chromen-2-one (PGC)

Yield 80%; mp 103–107 °C. ^1H NMR (CDCl_3 , 500 MHz, δ , TMS = 0): 3.22–3.24 (m, 1H, $-\text{CH}$ -propargylic), 4.92–4.94 (m, 2H, $-\text{CH}_2-$), 5.84 (d, 1H, J = 12 Hz, $-\text{CH}-$), 7.25–7.27 (m, 2H, ArH), 7.56 (s, 1H, ArH), 7.77 (d, 1H, J = 8 Hz, ArH). ^{13}C NMR (CDCl_3 , 125 MHz, δ , TMS = 0): 57.38,

76.50, 79.32, 91.71, 115.39, 116.60, 123.16, 124.28, 132.83, 153.17, 162.02, 164.24.

General procedure for the synthesis of 1-(2-bromoalkyl)indoline-2,3-diones

Indoline-2,3-dione (1 eq) was dissolved in DMF (in minimum amount), dibromoalkane (1 eq) and K_2CO_3 (1.5 eq) were added. The reaction mixture was stirred at room temperature. After the completion of the reaction as confirmed by TLC, the reaction mixture was poured on crushed ice. The impure product so obtained was filtered, air-dried, and subjected to column chromatography (hexane/ethyl acetate as eluent) to gain the desired product. All the other 1-bromoalkylindoline-2,3-diones were synthesized via the same procedure as mentioned above using various dibromoalkanes.

General procedure for the synthesis of 1-(4-azidoalkyl)indoline-2,3-diones (IBA)

In a minimum amount of DMF, 1-(4-Bromoalkyl)indoline-2,3-dione (1 eq) were dissolved and sodium azide (1 eq) was added and the mixture was stirred at room temperature. After the completion of the reaction, the reaction mixture was poured on crushed ice and precipitates (1-(4-azidoalkyl)indoline-2,3-diones) thus obtained were collected by simple filtration.

All the other 1-azidoalkylindoline-2,3-dione analogues were synthesized by following the above-mentioned procedure.

General procedure for the synthesis of triazole linked indoline-2,3-dione-coumarin hybrids

In DMF, 1-azidoalkylindoline-2,3-dione (1 eq) and 4-(prop-2-ynyloxy)-2H-chromen-2-one (PHC) (1 eq) were dissolved. The catalytic amount of pentahydrate copper sulphate ($\text{CuSO}_4 \cdot 5\text{H}_2\text{O}$) and its reducing agent, sodium ascorbate were added in it. Reaction mixture was kept aside for some time, at room temperature. After the completion of reaction as confirmed by TLC, the reaction mixture was filtered directly on crushed ice to remove the excess of CuSO_4 and sodium ascorbate. The solidified final product thus obtained was filtered and air-dried. The physical data of all the synthesized bi-functional hybrids is given below:

1-(2-(4-((2-oxo-2H-chromen-4-yl)oxy)methyl)-1H-1,2,3-triazol-1-yl)ethyl)indoline-2,3-dione (K-1): Yield 78%, mp 104–108 °C. ^1H NMR (d_6 -DMSO, 300 MHz, δ , TMS = 0): 4.21 (s, 2H, $-\text{CH}_2-$), 4.77 (s, 2H, $-\text{CH}_2-$), 5.38 (s, 2H, $-\text{CH}_2-$), 6.11 (s, 1H, $-\text{CH}-$), 6.91 (d, 1H, J = 7.8 Hz, ArH), 7.08 (t, 1H, ArH, J = 7.5 Hz), 7.41–7.46 (m, 2H, ArH), 7.54–7.56

(m, 2H, ArH), 7.68–7.71 (m, 2H, ArH), 8.49 (s, 1H, ArH). ^{13}C NMR (d_6 -DMSO, 125 MHz, δ , TMS = 0): 47.64, 62.93, 91.50, 110.52, 115.43, 116.84, 117.64, 123.29, 123.79, 124.64, 125.00, 133.33, 138.59, 150.54, 153.11, 158.55, 162.14, 164.73, 183.32. Anal.Calcd for $\text{C}_{22}\text{H}_{16}\text{N}_4\text{O}_5$: C, 63.46; H, 3.87; N, 13.46 Found: C, 63.26; H, 3.98; N, 13.15.

1-(2-(4-((2-oxo-2H-chromen-4-yloxy)methyl)-1H-1,2,3-triazol-1-yl)ethyl)-5-fluoroindoline-2,3-dione (K-2): Yield 79%, mp 74–78 °C. ^1H NMR (d_6 -DMSO, 300 MHz, δ , TMS = 0): 4.22 (s, 2H, $-\text{CH}_2-$), 4.76 (s, 2H, $-\text{CH}_2-$), 5.39 (s, 2H, $-\text{CH}_2-$), 6.14 (s, 1H, $-\text{CH}-$), 6.94 (s, 1H, ArH), 7.40–7.47 (m, 4H, ArH), 7.69–7.71 (m, 2H, ArH), 8.51 (s, 1H, ArH). ^{13}C NMR (d_6 -DMSO, 125 MHz, δ , TMS = 0): 47.61, 63.06, 79.06, 79.32, 79.58, 91.60, 111.80, 112.00, 112.07, 115.45, 116.87, 118.58, 118.64, 123.22, 124.60, 133.28, 146.86, 153.16, 158.59, 162.03, 164.72, 182.73. Anal.Calcd for $\text{C}_{22}\text{H}_{15}\text{FN}_4\text{O}_5$: C, 60.83; H, 3.48; F, 4.37; N, 12.90 Found: C, 60.52; H, 3.50; F, 4.21; N, 12.96.

1-(2-(4-((2-oxo-2H-chromen-4-yloxy)methyl)-1H-1,2,3-triazol-1-yl)ethyl)-5-chloroindoline-2,3-dione (K-3): Yield 79%, mp 160–164 °C. ^1H NMR (d_6 -DMSO, 500 MHz, δ , TMS = 0): 4.16 (s, 2H, $-\text{CH}_2-$), 4.70 (s, 2H, $-\text{CH}_2-$), 5.34 (s, 2H, $-\text{CH}_2-$), 6.09 (s, 1H, $-\text{CH}-$), 6.88 (d, 1H, J = 8.5 Hz, ArH), 7.35–7.40 (m, 2H, ArH), 7.56–7.57 (m, 2H, ArH), 7.64–7.67 (m, 2H, ArH), 8.45 (s, 1H, ArH). ^{13}C NMR (d_6 -DMSO, 125 MHz, δ , TMS = 0): 47.59, 63.15, 91.68, 112.35, 115.49, 116.90, 119.13, 123.23, 124.48, 124.66, 126.67, 128.02, 133.26, 137.35, 149.19, 153.20, 158.34, 161.99, 164.74, 182.25. Anal.Calcd for $\text{C}_{22}\text{H}_{15}\text{ClN}_4\text{O}_5$: C, 58.61; H, 3.35; Cl, 7.86; N, 12.43 Found: C, 58.33; H, 3.54; Cl, 7.77; N, 12.55.

1-(2-(4-((2-oxo-2H-chromen-4-yloxy)methyl)-1H-1,2,3-triazol-1-yl)ethyl)-5-bromoindoline-2,3-dione (K-4): Yield 83%, mp 74–78 °C. ^1H NMR (d_6 -DMSO, 500 MHz, δ , TMS = 0): 4.15 (s, 2H, $-\text{CH}_2-$), 4.70 (s, 2H, $-\text{CH}_2-$), 5.34 (s, 2H, $-\text{CH}_2-$), 6.10 (s, 1H, $-\text{CH}-$), 6.84 (d, 1H, J = 8 Hz, ArH), 7.37–7.41 (m, 2H, ArH), 7.65–7.71 (m, 4H, ArH), 8.44 (s, 1H, ArH). ^{13}C NMR (d_6 -DMSO, 125 MHz, δ , TMS = 0): 47.55, 63.15, 91.69, 112.80, 115.52, 116.92, 119.52, 123.26, 124.71, 126.56, 127.24, 133.29, 140.17, 149.57, 153.21, 155.86, 162.02, 164.77, 182.12. Anal. Calcd for $\text{C}_{22}\text{H}_{15}\text{BrN}_4\text{O}_5$: C, 53.35; H, 3.05; Br, 16.13; N, 11.31 Found: C, 53.44; H, 3.01; Br, 16.33; N, 11.12.

1-(2-(4-((2-oxo-2H-chromen-4-yloxy)methyl)-1H-1,2,3-triazol-1-yl)ethyl)-5-iodoindoline-2,3-dione (K-5): Yield 81%, mp 88–91 °C. ^1H NMR (d_6 -DMSO, 500 MHz, δ , TMS = 0): 4.17 (s, 2H, $-\text{CH}_2-$), 4.68 (s, 2H, $-\text{CH}_2-$), 5.37 (s, 2H, $-\text{CH}_2-$), 6.08 (s, 1H, $-\text{CH}-$), 6.82 (d, 1H, J = 8 Hz, ArH), 7.35–7.39 (m, 2H, ArH), 7.63–7.65 (m, 2H, ArH),

7.84–7.87 (m, 2H, ArH), 8.61 (s, 1H, ArH). ^{13}C NMR (d_6 -DMSO, 125 MHz, δ , TMS = 0): 47.59, 63.23, 91.74, 112.86, 115.57, 116.91, 119.59, 123.24, 124.70, 126.53, 127.30, 133.34, 140.19, 149.52, 153.27, 155.90, 161.97, 164.73, 182.53. Anal.Calcd for $\text{C}_{22}\text{H}_{15}\text{IN}_4\text{O}_5$: C, 48.73; H, 2.79; I, 23.40; N, 10.33 Found: C, 48.93; H, 2.68; I, 23.44; N, 10.22.

1-(2-(4-((2-oxo-2H-chromen-4-yloxy)methyl)-1H-1,2,3-triazol-1-yl)ethyl)-5-nitroindoline-2,3-dione (K-6): Yield 83%, mp 104–108 °C. ^1H NMR (d_6 -DMSO, 500 MHz, δ , TMS = 0): 4.14 (s, 2H, $-\text{CH}_2-$), 4.65 (s, 2H, $-\text{CH}_2-$), 5.37 (s, 2H, $-\text{CH}_2-$), 6.11 (s, 1H, $-\text{CH}-$), 6.83 (s, 1H, ArH), 7.41–7.44 (m, 2H, ArH), 7.61–7.64 (m, 2H, ArH), 7.96–7.99 (m, 2H, ArH), 8.76 (s, 1H, ArH). ^{13}C NMR (d_6 -DMSO, 125 MHz, δ , TMS = 0): 47.71, 63.32, 91.65, 112.82, 115.55, 116.96, 119.62, 123.43, 124.76, 126.52, 127.13, 135.33, 146.56, 152.43, 153.86, 155.95, 162.45, 164.78, 182.72. Anal. Calcd for $\text{C}_{22}\text{H}_{15}\text{N}_5\text{O}_7$: C, 57.27; H, 3.28; N, 15.18 Found: C, 57.42; H, 3.13; N, 15.45.

1-(2-(4-((2-oxo-2H-chromen-4-yloxy)methyl)-1H-1,2,3-triazol-1-yl)ethyl)-5-methoxyindoline-2,3-dione (K-7): Yield 75%, mp 70–74 °C. ^1H NMR (d_6 -DMSO, 300 MHz, δ , TMS = 0): 3.68 (s, 3H, $-\text{OCH}_3$), 4.12 (s, 2H, $-\text{CH}_2-$), 4.69 (s, 2H, $-\text{CH}_2-$), 5.32 (s, 2H, $-\text{CH}_2-$), 6.06 (s, 1H, $-\text{CH}-$), 6.80 (d, 1H, J = 8.0 Hz, ArH), 7.07–7.09 (m, 2H, ArH), 7.33–7.39 (m, 2H, ArH), 7.63–7.66 (m, 2H, ArH), 8.42 (s, 1H, ArH). ^{13}C NMR (d_6 -DMSO, 125 MHz, δ , TMS = 0): 47.61, 56.24, 63.06, 91.57, 109.50, 111.73, 112.08, 115.45, 116.87, 118.19, 123.26, 124.44, 124.64, 126.59, 133.30, 144.45, 153.67, 156.15, 158.61, 162.08, 164.77, 183.56. Anal.Calcd for $\text{C}_{23}\text{H}_{18}\text{N}_4\text{O}_6$: C, 61.88; H, 4.06; N, 12.55 Found: C, 60.99; H, 4.23; N, 12.32.

1-(3-(4-((2-oxo-2H-chromen-4-yloxy)methyl)-1H-1,2,3-triazol-1-yl)propyl)indoline-2,3-dione (L-1): Yield 76%, mp 122–125 °C. ^1H NMR (d_6 -DMSO, 300 MHz, δ , TMS = 0): 2.23 (s, 2H, $-\text{CH}_2-$), 3.75 (s, 2H, $-\text{CH}_2-$), 4.52 (s, 2H, $-\text{CH}_2-$), 5.41 (s, 2H, $-\text{CH}_2-$), 6.15 (s, 1H, $-\text{CH}-$), 7.11–7.18 (m, 2H, ArH), 7.32–7.41 (m, 2H, ArH), 7.54–7.75 (m, 4H, ArH), 8.37 (s, 1H, ArH). ^{13}C NMR (d_6 -DMSO, 125 MHz, δ , TMS = 0): 28.00, 37.36, 47.71, 63.29, 91.78, 110.97, 115.54, 116.94, 118.19, 123.25, 123.61, 124.70, 124.89, 125.81, 133.31, 138.45, 150.84, 153.23, 158.82, 162.03, 164.82, 183.74. Anal.Calcd for $\text{C}_{23}\text{H}_{18}\text{N}_4\text{O}_5$: C, 64.18; H, 4.22; N, 13.02 Found: C, 64.33; H, 4.11; N, 13.41.

1-(3-(4-((2-oxo-2H-chromen-4-yloxy)methyl)-1H-1,2,3-triazol-1-yl)propyl)-5-fluoroindoline-2,3-dione (L-2): Yield 79%, mp 94–97 °C. ^1H NMR (d_6 -DMSO, 300 MHz, δ , TMS = 0): 2.18 (s, 2H, $-\text{CH}_2-$), 4.19 (s, 2H, $-\text{CH}_2-$), 4.77 (s, 2H, $-\text{CH}_2-$), 5.37 (s, 2H, $-\text{CH}_2-$), 6.15 (s, 1H, $-\text{CH}-$), 6.93

(s, 1H, ArH), 7.43–7.48 (m, 4H, ArH), 7.70–7.74 (m, 2H, ArH), 8.50 (s, 1H, ArH). ^{13}C NMR (d_6 -DMSO, 125 MHz, δ , TMS = 0): 28.87, 47.56, 63.21, 79.32, 79.31, 79.54, 91.66, 111.83, 112.12, 112.21, 115.43, 116.82, 118.52, 118.59, 123.32, 124.64, 133.19, 146.82, 153.14, 158.73, 162.23, 164.69, 183.74. Anal.Calcd for $\text{C}_{23}\text{H}_{17}\text{FN}_4\text{O}_5$: C, 61.61; H, 3.82; F, 4.24; N, 12.49 Found: C, 61.45; H, 3.95; F, 4.06; N, 12.53.

1-(3-(4-((2-oxo-2H-chromen-4-yloxy)methyl)-1H-1,2,3-triazol-1-yl)propyl)-5-chloroindoline-2,3-dione (L-3): Yield 71%, mp 166–169 °C. ^1H NMR (d_6 -DMSO, 500 MHz, δ , TMS = 0): 2.20 (s, 2H, $-\text{CH}_2-$), 3.74 (s, 2H, $-\text{CH}_2-$), 4.51 (s, 2H, $-\text{CH}_2-$), 5.41 (s, 2H, $-\text{CH}_2-$), 6.15 (s, 1H, $-\text{CH}-$), 7.03–7.04 (m, 1H, ArH), 7.34–7.41 (m, 2H), 7.66–7.96 (m, 4H, ArH), 8.35 (s, 1H, ArH). ^{13}C NMR (d_6 -DMSO, 125 MHz, δ , TMS = 0): 27.87, 37.40, 47.65, 63.30, 86.47, 91.78, 113.48, 115.54, 116.95, 123.35, 124.70, 125.76, 132.53, 133.32, 145.86, 150.17, 153.23, 158.17, 162.03, 164.83, 182.41. Anal.Calcd for $\text{C}_{23}\text{H}_{17}\text{ClN}_4\text{O}_5$: C, 59.43; H, 3.69; Cl, 7.63; N, 12.05 Found: C, 59.60; H, 3.55; Cl, 7.75; N, 12.01.

1-(3-(4-((2-oxo-2H-chromen-4-yloxy)methyl)-1H-1,2,3-triazol-1-yl)propyl)-5-bromoindoline-2,3-dione (L-4): Yield 80%, mp 74–78 °C. ^1H NMR (d_6 -DMSO, 500 MHz, δ , TMS = 0): 2.16 (s, 2H, $-\text{CH}_2-$), 4.17 (s, 2H, $-\text{CH}_2-$), 4.72 (s, 2H, $-\text{CH}_2-$), 5.35 (s, 2H, $-\text{CH}_2-$), 6.08 (s, 1H, $-\text{CH}-$), 6.86 (d, 1H, $J = 8$ Hz, ArH), 7.38–7.42 (m, 2H, ArH), 7.64–7.70 (m, 4H, ArH), 8.46 (s, 1H, ArH). ^{13}C NMR (d_6 -DMSO, 125 MHz, δ , TMS = 0): 28.66, 47.59, 63.12, 91.71, 112.89, 115.56, 116.97, 119.57, 123.29, 124.76, 126.58, 127.28, 133.32, 140.19, 149.59, 153.28, 155.89, 162.06, 164.79, 182.56. Anal.Calcd for $\text{C}_{23}\text{H}_{17}\text{BrN}_4\text{O}_5$: C, 54.24; H, 3.36; Br, 15.69; N, 11.00 Found: C, 54.28; H, 3.15; Br, 15.78; N, 11.03.

1-(3-(4-((2-oxo-2H-chromen-4-yloxy)methyl)-1H-1,2,3-triazol-1-yl)propyl)-5-iodoindoline-2,3-dione (L-5): Yield 83%, mp 98–102 °C. ^1H NMR (d_6 -DMSO, 500 MHz, δ , TMS = 0): 2.13 (s, 2H, $-\text{CH}_2-$), 4.14 (s, 2H, $-\text{CH}_2-$), 4.70 (s, 2H, $-\text{CH}_2-$), 5.35 (s, 2H, $-\text{CH}_2-$), 6.11 (s, 1H, $-\text{CH}-$), 6.81 (s, 1H, ArH), 7.36–7.39 (m, 2H, ArH), 7.65–7.68 (m, 2H, ArH), 7.80–7.84 (m, 2H, ArH), 8.59 (s, 1H, ArH). ^{13}C NMR (d_6 -DMSO, 125 MHz, δ , TMS = 0): 28.69, 47.65, 63.28, 91.72, 112.81, 115.54, 116.98, 119.63, 123.23, 124.72, 126.57, 127.33, 133.37, 140.14, 149.56, 153.24, 155.94, 161.94, 164.76, 182.63. Anal.Calcd for $\text{C}_{23}\text{H}_{17}\text{IN}_4\text{O}_5$: C, 49.66; H, 3.08; I, 22.81; N, 10.07 Found: C, 49.55; H, 2.88; I, 22.84; N, 10.01.

1-(3-(4-((2-oxo-2H-chromen-4-yloxy)methyl)-1H-1,2,3-triazol-1-yl)propyl)-5-nitroindoline-2,3-dione (L-6): Yield 79%, mp 106–109 °C. ^1H NMR (d_6 -DMSO, 500 MHz, δ ,

TMS = 0): 2.14 (s, 2H, $-\text{CH}_2-$), 4.15 (s, 2H, $-\text{CH}_2-$), 4.65 (s, 2H, $-\text{CH}_2-$), 5.34 (s, 2H, $-\text{CH}_2-$), 6.10 (s, 1H, $-\text{CH}-$), 6.83 (s, 1H, ArH), 7.42–7.45 (m, 2H, ArH), 7.61–7.67 (m, 3H, ArH), 7.97–7.99 (m, 1H, ArH), 8.76 (s, 1H, ArH). ^{13}C NMR (d_6 -DMSO, 125 MHz, δ , TMS = 0): 28.56, 47.73, 63.31, 91.64, 112.83, 115.56, 116.92, 119.65, 123.43, 124.77, 126.52, 127.16, 135.34, 146.53, 152.46, 153.82, 155.94, 162.55, 164.74, 182.72. Anal.Calcd for $\text{C}_{23}\text{H}_{17}\text{N}_5\text{O}_7$: C, 58.11; H, 3.60; N, 14.73 Found: C, 58.19; H, 3.51; N, 14.99.

1-(3-(4-((2-oxo-2H-chromen-4-yloxy)methyl)-1H-1,2,3-triazol-1-yl)propyl)-5-methoxyindoline-2,3-dione (L-7): Yield 76%, mp 87–90 °C. ^1H NMR (d_6 -DMSO, 300 MHz, δ , TMS = 0): 2.19–2.24 (m, 2H, $-\text{CH}_2-$), 3.71–3.76 (m, 3H, $-\text{OCH}_3$), 4.50–4.53 (m, 2H, $-\text{CH}_2-$), 5.41 (s, 2H, $-\text{CH}_2-$), 6.15 (s, 1H, $-\text{CH}-$), 7.10–7.14 (m, 2H, ArH), 7.21–7.23 (m, 1H, ArH), 7.32–7.41 (m, 2H, ArH), 7.64–7.75 (m, 2H, ArH), 8.37 (s, 1H, ArH). ^{13}C NMR (d_6 -DMSO, 125 MHz, δ , TMS = 0): 27.99, 36.26, 37.34, 47.71, 56.36, 63.30, 91.77, 109.76, 112.04, 115.54, 116.93, 118.68, 123.35, 124.09, 124.69, 133.31, 144.59, 153.22, 156.16, 158.82, 162.03, 164.83, 183.98. Anal.Calcd for $\text{C}_{24}\text{H}_{20}\text{N}_4\text{O}_6$: C, 62.60; H, 4.38; N, 12.17 Found: C, 62.66; H, 4.13; N, 12.34.

1-(4-(4-((2-oxo-2H-chromen-4-yloxy)methyl)-1H-1,2,3-triazol-1-yl)butyl)indoline-2,3-dione(M-1): Yield 74%, mp 146–150 °C. ^1H NMR (d_6 -DMSO, 500 MHz, δ , TMS = 0): 1.58–1.61 (m, 2H, $-\text{CH}_2-$), 1.92–1.95 (m, 2H, $-\text{CH}_2-$), 3.69–3.72 (m, 2H, $-\text{CH}_2-$), 4.44–4.47 (m, 2H, $-\text{CH}_2-$), 5.40 (s, 2H, $-\text{CH}_2-$), 6.14 (s, 1H, $-\text{CH}-$), 7.11–7.18 (m, 2H, ArH), 7.34–7.41 (m, 2H, ArH), 7.53 (d, 1H, $J = 7$ Hz, ArH), 7.63–7.66 (m, 2H, ArH), 7.73 (d, 1H, $J = 7.5$ Hz, ArH), 8.38 (s, 1H, ArH). ^{13}C NMR (d_6 -DMSO, 125 MHz, δ , TMS = 0): 24.25, 27.42, 49.53, 63.33, 91.77, 111.06, 115.54, 116.91, 118.01, 123.33, 123.58, 124.66, 124.90, 133.26, 138.51, 151.03, 153.22, 158.67, 161.98, 164.81, 183.86. Anal.Calcd for $\text{C}_{24}\text{H}_{20}\text{N}_4\text{O}_5$: C, 64.86; H, 4.54; N, 12.61 Found: C, 64.97; H, 4.32; N, 12.85.

1-(4-(4-((2-oxo-2H-chromen-4-yloxy)methyl)-1H-1,2,3-triazol-1-yl)butyl)-5-fluoroindoline-2,3-dione (M-2): Yield 77%, mp 110–114 °C. ^1H NMR (d_6 -DMSO, 300 MHz, δ , TMS = 0): 1.59 (s, 2H, $-\text{CH}_2-$), 1.87 (s, 2H, $-\text{CH}_2-$), 3.70 (s, 2H, $-\text{CH}_2-$), 4.44 (s, 2H, $-\text{CH}_2-$), 5.34 (s, 2H, $-\text{CH}_2-$), 6.13 (s, 1H, $-\text{CH}_2-$), 6.91 (s, 1H, $-\text{CH}-$), 7.44–7.49 (m, 4H, ArH), 7.72–7.74 (m, 2H, ArH), 8.52 (s, 1H, ArH). ^{13}C NMR (d_6 -DMSO, 125 MHz, δ , TMS = 0): 24.44, 27.34, 47.52, 63.25, 79.32, 79.38, 79.53, 91.65, 111.83, 112.11, 112.29, 115.42, 116.81, 118.55, 118.68, 123.32, 124.61, 133.23, 146.81, 153.15, 158.77, 162.19, 164.71, 183.72. Anal.Calcd for $\text{C}_{24}\text{H}_{19}\text{FN}_4\text{O}_5$: C, 62.34; H, 4.14; F, 4.11; N, 12.12 Found: C, 62.62; H, 4.25; F, 3.99; N, 12.19.

1-(4-(4-((2-oxo-2H-chromen-4-yloxy)methyl)-1H-1,2,3-triazol-1-yl)butyl)-5-chloroindoline-2,3-dione (M-3): Yield 70%, mp 170–172 °C. ¹H NMR (d₆-DMSO, 500 MHz, δ, TMS = 0): 1.56 (s, 2H, -CH₂-), 1.92 (s, 2H, -CH₂-), 3.68 (s, 2H, -CH₂-), 4.44 (s, 2H, -CH₂-), 5.39 (s, 2H, -CH₂-), 6.13 (s, 1H, -CH-), 7.20–7.40 (m, 3H, ArH), 7.56–7.73 (m, 4H, ArH), 8.39 (s, 1H, ArH). ¹³C NMR (d₆-DMSO, 125 MHz, δ, TMS = 0): 24.14, 27.30, 49.56, 63.37, 91.75, 112.75, 115.52, 116.89, 119.43, 123.33, 124.37, 124.67, 127.79, 133.27, 137.29, 149.53, 153.20, 158.46, 162.01, 164.82, 182.75. Anal.Calcd for C₂₄H₁₉ClN₄O₅: C, 60.19; H, 4.00; Cl, 7.40; N, 11.70 Found: C, 60.30; H, 3.88; Cl, 7.47; N, 11.64.

1-(4-(4-((2-oxo-2H-chromen-4-yloxy)methyl)-1H-1,2,3-triazol-1-yl)butyl)-5-bromoindoline-2,3-dione (M-4): Yield 76%, mp 75–80 °C. ¹H NMR (d₆-DMSO, 500 MHz, δ, TMS = 0): 1.57 (s, 2H, -CH₂-), 1.92 (s, 2H, -CH₂-), 3.69 (s, 2H, -CH₂-), 4.44 (s, 2H, -CH₂-), 5.40 (s, 2H, -CH₂-), 6.14 (s, 1H, -CH-), 7.16 (s, 1H, ArH), 7.34–7.41 (m, 2H, ArH), 7.66–7.80 (m, 4H, ArH), 8.38 (s, 1H, ArH). ¹³C NMR (d₆-DMSO, 125 MHz, δ, TMS = 0): 24.13, 27.31, 49.55, 63.36, 88.90, 91.77, 113.20, 115.27, 115.53, 116.91, 119.83, 123.34, 124.46, 127.10, 133.27, 140.09, 147.92, 153.21, 158.30, 161.99, 164.81, 182.61. Anal.Calcd for C₂₄H₁₉BrN₄O₅: C, 55.08; H, 3.66; Br, 15.27; N, 10.71 Found: C, 55.25; H, 3.44; Br, 15.45; N, 10.55.

1-(4-(4-((2-oxo-2H-chromen-4-yloxy)methyl)-1H-1,2,3-triazol-1-yl)butyl)-5-iodoindoline-2,3-dione (M-5): Yield 83%, mp 97–102 °C. ¹H NMR (d₆-DMSO, 500 MHz, δ, TMS = 0): 1.58 (s, 2H, -CH₂-), 1.91 (s, 2H, -CH₂-), 3.71 (s, 2H, -CH₂-), 4.44 (s, 2H, -CH₂-), 5.38 (s, 2H, -CH₂-), 6.08 (s, 1H, -CH-), 6.84 (s, 1H, ArH), 7.34–7.37 (m, 2H, ArH), 7.67–7.69 (m, 2H, ArH), 7.76–7.79 (m, 2H, ArH), 8.61 (s, 1H, ArH). ¹³C NMR (d₆-DMSO, 125 MHz, δ, TMS = 0): 24.54, 27.43, 48.99, 63.56, 91.76, 112.82, 115.58, 117.12, 119.67, 123.25, 124.77, 126.53, 127.33, 133.32, 140.11, 149.45, 153.00, 155.95, 161.94, 164.71, 182.73. Anal. Calcd for C₂₄H₁₉IN₄O₅: C, 50.54; H, 3.36; I, 22.25; N, 9.82 Found: C, 50.51; H, 3.45; I, 22.12; N, 10.00.

1-(4-(4-((2-oxo-2H-chromen-4-yloxy)methyl)-1H-1,2,3-triazol-1-yl)butyl)-5-nitroindoline-2,3-dione (M-6): Yield 80%, mp 110–112 °C. ¹H NMR (d₆-DMSO, 500 MHz, δ, TMS = 0): 1.57 (s, 2H, -CH₂-), 1.92 (s, 2H, -CH₂-), 3.66 (s, 2H, -CH₂-), 4.43 (s, 2H, -CH₂-), 5.37 (s, 2H, -CH₂-), 6.10 (s, 1H, -CH-), 6.84 (s, 1H, ArH), 7.44–7.47 (m, 2H, ArH), 7.62–7.67 (m, 2H, ArH), 7.94–7.96 (m, 2H, ArH), 8.72 (s, 1H, ArH). ¹³C NMR (d₆-DMSO, 125 MHz, δ, TMS = 0): 24.34, 27.65, 48.56, 63.65, 91.34, 112.87, 115.52, 116.97, 119.63, 123.46, 124.73, 126.55, 127.12, 135.35, 146.56, 152.43, 153.84, 155.96, 162.53, 164.77, 182.69. Anal.

Calcd for C₂₄H₁₉N₅O₇: C, 58.90; H, 3.91; N, 14.31 Found: C, 58.99; H, 3.76; N, 14.42.

1-(4-(4-((2-oxo-2H-chromen-4-yloxy)methyl)-1H-1,2,3-triazol-1-yl)butyl)-5-methoxyindoline-2,3-dione (M-7): Yield 73%, mp 97–100 °C. ¹H NMR (d₆-DMSO, 300 MHz, δ, TMS = 0): 1.57 (s, 2H, -CH₂-), 1.92 (s, 2H, -CH₂-), 3.67 (s, 2H, -CH₂-), 3.75 (s, 3H, -OCH₃), 4.44 (s, 2H, -CH₂-), 5.39 (s, 2H, -CH₂-), 6.13 (s, 1H, -CH-), 7.09–7.11 (m, 2H, ArH), 7.20–7.22 (m, 1H, ArH), 7.33–7.35 (m, 1H, ArH), 7.39–7.40 (m, 1H, ArH), 7.65–7.67 (m, 1H, ArH), 7.72–7.73 (m, 1H, ArH), 8.37 (s, 1H, ArH). ¹³C NMR (d₆-DMSO, 125 MHz, δ, TMS = 0): 24.23, 27.39, 49.53, 56.35, 63.32, 91.74, 109.78, 112.13, 115.52, 116.90, 118.18, 123.33, 124.23, 124.68, 125.58, 133.28, 144.78, 153.20, 156.14, 158.67, 162.02, 164.83, 184.12. Anal.Calcd for C₂₅H₂₂N₄O₆: C, 63.29; H, 4.67; N, 11.81 Found: C, 63.45; H, 4.47; N, 11.92.

In vitro xanthine oxidase assay

All the synthesized compounds were evaluated against XO enzyme. Bovine milk XO (grade 1, ammonium sulfate suspension, Sigma-Aldrich, India) activity was assayed spectrophotometrically by measuring the UA formation at 293 nm using a Hitachi U-3010 UV-visible spectrophotometer at 25 °C. The reaction mixture contains 50 mM potassium phosphate buffer (pH 7.6), 75 μM xanthine, and 0.08 units of XO. Inhibition of XO activity of synthetics at different concentrations (1, 5, 10, 25, 50 μM) was measured by following the decrease in the UA formation at 293 nm at 25 °C. The enzyme was pre-incubated for 5 min with a test compound, dissolved in DMSO (1% v/v), and the reaction was started by the addition of xanthine. The final concentration of DMSO (1% v/v) did not interfere with the enzyme activity. All the experiments were performed in triplicate and values were expressed as the mean of three experiments (Escribano et al. 1988; Takano et al. 2005).

Enzyme kinetics study

Potent XO enzyme inhibitors were further investigated for the type of inhibition and enzyme kinetics study was carried out. The Lineweaver–Burk plot was established from which we could calculate the K_m, V_{max} of the slope of inhibitor and the value of α (a constant that defines the degree to which inhibitor binding affects the affinity of the enzyme for substrate (Copeland 2005)).

Molecular modeling studies

Crystal structure of XO (PDB entry: 1N5X; resolution 2.8 Å) was downloaded from Protein Data Bank.

Preparation of structure was done by using drug design platform LeadIT. Co-crystallized ligand Febuxostat was used for defining binding site with the radius of 6.50 Å. Structure of compound was drawn on ChemDraw Ultra (2013) and its energy was minimized by employing MM2 force field in Chem 3D Ultra software. Prepared compound was used as protonated in aqueous solution and docked into prepared binding site using FlexX docking module in LeadIT. All FlexX solutions obtained were scored using a consensus scoring function (CScore) and ranked accordingly. Top best pose with the highest score was selected for investigation of interactions. 3D enzyme-hybrid interactions were visualized using Discovery Studio Visualizer: Biovia 2016.

Acknowledgements Authors are grateful to the University Grants Commission for providing funds under Rajiv Gandhi National Fellowship (RGNF) and National Fellowships for Other Backward Classes (NFOBC), Department of Science & Technology (DST-PURSE), Council of Scientific and Industrial Research (CSIR): Project no. 02(0319)17/EMR-II, Women Scientists Scheme-A (WOS-A: DST) and DST-FIST. The authors are also thankful to Guru Nanak Dev University, Amritsar for providing various basic facilities to carry out the research work.

Compliance with ethical standards

Conflict of interest The authors declare that they have no conflict of interest.

Publisher's note Springer Nature remains neutral with regard to jurisdictional claims in published maps and institutional affiliations.

References

- Ali HI, Fujita T, Akaho E, Nagamatsu T (2010) A comparative study of AutoDock and PMF scoring performances, and SAR of 2-substituted pyrazolotriazolopyrimidines and 4-substituted pyrazolopyrimidines as potent xanthine oxidase inhibitors. *J Comput Aided Mol Des* 24:57–75
- Becker MA, Kisicki J, Khosravan R, Wu J, Mulford D, Hunt B, MacDonald P, Joseph-Ridge N (2004) Febuxostat (TMX-67), a novel, non-purine, selective inhibitor of xanthine oxidase, is safe and decreases serum urate in healthy volunteers. *Nucl Nucl Nucl* 23:35–40
- Becker M, Schumacher H, MacDonald PA (2007) Febuxostat: a guide to its use in chronic hyperuricaemia. *Abstr no 757 Arthritis Rheum* 56(9 Suppl):S322
- Biagi G, Giorgi I, Pacchini F, Livi O, Scartoni V (2001) 2-Alkylalkoxyalkylthiohypoxanthines as new potent inhibitors of xanthine oxidase. *Farmaco* 56:809–813
- Borges F, Fernandes E, Roleira F (2002) Progress towards the discovery of xanthine oxidase inhibitors. *Curr Med Chem* 9:195–217
- Brien DE, Springer RH, Albert TNA, Senga K, Miller JP, Streeter DG (1985) Purine analog inhibitors of xanthine oxidase - structure activity relationships and proposed binding of the molybdenum cofactor. *J Heterocycl Chem* 22:601–634
- ChemDraw Ultra 6.0 and Chem3D Ultra (2013); Cambridge Software Corporation: Cambridge, USA
- Chen C, Huang C, Tsai K, Huang W, Huang W, Hsu Y, Hsu F (2014) Evaluation of the antihyperuricemic activity of phytochemicals from *davallia formosana* by enzyme assay and hyperuricemic mice model. *Evid Based Complement Alternat Med* 2014:1–8
- Copeland RA (2005) *Evaluation of Enzyme Inhibitors in Drug Discovery*. Wiley, Hoboken
- Dassault Systemes BIOVIA (2016) *Discovery studio modeling environment*, release 2017. Dassault Systemes, San Diego
- Dhiman R, Sharma S, Singh G, Nepali K, Bedi PMS (2012) Design and synthesis of aza-flavones as a new class of xanthine oxidase inhibitors. *Arch Pharm Chem Life Sci* 346:7–16
- Escribano J, Gracia-Canovas F, Garcia-Carmona F (1988) A kinetic study of hypoxanthine oxidation by milk xanthine oxidase. *Bio Chem J* 254:829–833
- Fais A, Era B, Asthana S, Sogos V, Medda R, Santana L, Uriarte E, Mtos MJ, Delogu F, Kumar A (2018) Coumarin derivatives as promising xanthine oxidase inhibitors. *Ijbiomac* 120:1286–1293
- Hille R (2006) Structure and function of xanthine oxidoreductase. *Eur J Inorg Chem* 10:1913–1926
- Ishibuchi S, Morimoto H, Oe T, Ikebe T, Inoue H, Fukunari A, Kamezawa M, Yamada I, Naka Y (2001) Synthesis and structure–activity relationships of 1-Phenylpyrazoles as xanthine oxidase inhibitors. *Bioorg Med Chem Lett* 11:879–882
- Kaur C, Dhiman S, Singh H, Kaur M, Bhagat S, Gupta M, Sharma S, Bedi PMS (2015) Synthesis, screening and docking studies of benzochromone derivatives as xanthine oxidase inhibitors. *J Chem Phar Res* 7:127–136
- Kaur G, Singh JV, Gupta MK, Bhagat K, Gulati HK, Singh A, Bedi PMS, Singh H, Sharma S (2019) Thiazole-5-carboxylic acid derivatives as potent xanthine oxidase inhibitors: design, synthesis, *in vitro* evaluation, and molecular modeling studies. *Medicinal Chem Res* 29:83–93
- Kaur M, Kaur A, Mankotia S, Singh H, Singh A, Singh JV, Gupta MK, Sharma S, Nepali K, Bedi PMS (2017) Synthesis, screening and docking of fused pyrano[3,2-d]pyrimidine derivatives as xanthine oxidase inhibitor. *Eur J Med Chem* 131:14–28
- Kaur R, Naaz F, Sharma S, Mehndiratta S, Gupta MK, Bedi PMS, Nepali K (2015) Screening of a library of 4-aryl/heteroaryl-4H-fused pyrans for xanthine oxidase inhibition: synthesis, biological evaluation and docking studies. *Med Chem Res* 24:3334–3349
- Komoriya K, Osada Y, Hasegawa M, Horiuchi H, Kondo S, Couch RC, Griffin TB (1993) Hypouricemic effect of allopurinol and the novel xanthine oxidase inhibitor TEI-6720 in chimpanzees. *Eur J Pharm* 250:455–460
- Kumar R, Darpan, Sharma S, Singh R (2011) Xanthine oxidase inhibitors: a patent survey. *Expert Opin Ther Pat* 21:1071–1108
- Love BL, Barrons R, Veverka A, Snider KM (2010) Urate-lowering therapy for gout: focus on febuxostat. *Pharmacother* 30:594–608
- Malik N, Dhiman P, Sobarzo-Sanchez E, Khatkar A (2018) Flavonoids and anthraquinones as xanthine oxidase and monoamine oxidase inhibitors: a new approach towards inflammation and oxidative stress. *Curr Top Med Chem* 18:2154–2164
- Mehmood A, Ishaq M, Zhao L, Safdar B, Rehman AU, Munir M, Raza A, Nadeem M, Iqbal W, Wang C (2019) Natural compounds with xanthine oxidase inhibitory activity: a review. *Chem Biol Drug Des* 93:387–418
- Nagamatsu T, Fujita T, Endo K (2000) Novel xanthine oxidase inhibitor studies. Part 2. Synthesis and xanthine oxidase inhibitory activities of 2-substituted 6-alkylidenhydrazino- or 6-arylmethylidenhydrazino-7H-purines and 3- and/or 5-substituted 9H-1,2,4-triazolo[3,4-i]purines. *Perkin Trans* 1:33–38
- Nagamatsu T, Ukai M, F, Yoneda F, Brown DJ (1985) Syntheses of 4-methyl-s-triazolo[4,3-a]purin-9(4H)-ones and tetrazolo-[1,5-a]purin-9(4H)-ones as Aza Analogs of “Y” Bases. *Chem Pharm Bull* 33:3113–3121

- Nagamatsu T, Yamasaki H (1995) Facile, general and productive syntheses of the fluorescent wye (4,9-dihydro-4,6-dimethyl-9-oxo-1H-imidazo[1,2-a]purine) in phenylalanine tRNA, its 2-substituted derivatives and 7-aza analogues. *J Chem Soc Chem Commun* 19:2041–2043
- Oetl K, Reibneggar G (1999) Pteridines as inhibitors of xanthine oxidase: structural requirements. *Biochim Biophys Acta* 1430:387–395
- Ojha R, Singh J, Ojha A, Singh H, Sharma S, Nepali K (2017) An updated patent review: xanthine oxidase inhibitors for the treatment of hyperuricemia and gout (2011–2015). *Expert Opin Ther Pat* 27:311–345
- Osada Y, Tsuchimoto M, Fukushima H, Takahashi K, Kondo S, Hasegawa M, Komoriya K (1993) Hypouricemic effect of the novel xanthine oxidase inhibitor, TEI-6720, in rodents. *Eur J Pharm* 241:183–188
- Pacher P, Nivorozhkin A, Szabo C (2006) Therapeutic effects of xanthine oxidase inhibitors: renaissance half a century after the discovery of allopurinol. *Pharm Rev* 58:87–114
- Pascart T, Richette P (2018) Investigational drugs for hyperuricemia, an update on recent developments. *Expert Opin Inv Drug* 27:437–444
- Schumacher HRJ, Becker MA, Wortmann RL, Macdonald PA, Hunt B, Streit J, Lademacher C, Joseph-Ridge N (2008) Effects of febuxostat versus allopurinol and placebo in reducing serum urate in subjects with hyperuricemia and gout: a 28-week, phase III, randomized, double-blind, parallel-group trial. *Arthritis Rheum* 59:1540–1548
- Sebastian E, Sattui, Gaffo AL (2016) Treatment of hyperuricemia in gout: current therapeutic options, latest developments and clinical implications. *Ther Adv Musculoskel Dis* 8:145–159
- Singh JV, Mal G, Kaur G, Gupta MK, Singh A, Nepali K, Singh H, Sharma S, Bedi PMS (2019) Benzoflavone derivatives as potent antihyperuricemic agents. *Med Chem Commun* 10:128–147
- Sharma S, Sharma K, Ojha R, Kumar D, Singh G, Nepali K, Bedi PMS (2014) Microwave assisted synthesis of naphthopyrans catalysed by silica supported fluoroboric acid as a new class of non purine xanthine oxidase inhibitors. *Bioorg Med Chem Lett* 24:495–500
- Shukla S, Kumar D, Ojha R, Gupta MK, Nepali K, Bedi PMS (2014) 4,6-Diaryl/heteroarylpyrimidin-2(1H)-ones as a new class of xanthine oxidase inhibitors. *Arch Pharm Chem Life Sci* 347:1–10
- Strilchuk L, Fogacci F, Cicero AF (2019) Safety and tolerability of available urate-lowering drugs: a critical review. *Expert Opin Drug Saf* 18:261–271
- Takano Y, Hase-Aoki K, Horiuchi H, Zhao L, Kasahara Y, Kondo S, Becker MA (2005) Selectivity of febuxostat, a novel non-purine inhibitor of xanthine oxidase/xanthine dehydrogenase. *Life Sci* 76:1835–1847
- Virdi HS, Sharma S, Mehndiratta S, Bedi PMS, Nepali K (2014) Design, synthesis and evaluation of 2,4-diarylpyrano[3,2-c]chromen-5(4H)-one as a new class of non-purine xanthine oxidase inhibitors. *J Enzym Inhib Med Chem* 30:1–7
- Wortmann RL (1998) Gout and other disorders of purine metabolism. In: Brunwald E ed. *Harrison's principles of internal medicine*. McGraw-Hill, New York (NY), Vol. 14, p 2158–2166



New coumarin-benzotriazole based hybrid molecules as inhibitors of acetylcholinesterase and amyloid aggregation

Atamjit Singh^a, Sahil Sharma^a, Saroj Arora^b, Shivani Attri^b, Prabhjot Kaur^b, Harmandeep Kaur Gulati^a, Kavita Bhagat^a, Nitish Kumar^a, Harbinder Singh^{a,*}, Jatinder Vir Singh^{a,*}, Preet Mohinder Singh Bedi^{a,*}

^a Department of Pharmaceutical Sciences, Guru Nanak Dev University, Amritsar, Punjab 143005, India

^b Department of Botanical and Environmental Sciences, Guru Nanak Dev University, Amritsar, Punjab 143005, India

ARTICLE INFO

Keywords:

Alzheimer's disease
Coumarin-benzotriazole hybrids
Acetylcholinesterase inhibitors
Amyloid aggregation inhibitor
Molecular docking

ABSTRACT

A novel series of triazole tethered coumarin-benzotriazole hybrids based on donepezil skeleton has been designed and synthesized as multifunctional agents for the treatment of Alzheimer's disease (AD). Among the synthesized compounds **13b** showed most potent acetylcholinesterase (AChE) inhibition ($IC_{50} = 0.059 \mu M$) with mixed type inhibition scenario. Structure-activity relationship revealed that three-carbon alkyl chain connecting coumarin and triazole is well tolerable for inhibitory potential. Hybrids obtained from 4-hydroxycoumarin and 1-benzotriazole were most potent AChE inhibitors. The inhibitory potential of all compounds against butyrylcholinesterase was also evaluated but all showed negligible activity suggesting that the hybrid molecules are selective AChE inhibitors. **13b** (most potent AChE inhibitor) also showed copper-induced $A\beta_{1-42}$ aggregation inhibition (34.26% at $50 \mu M$) and chelating properties for metal ions (Cu^{2+} , Fe^{2+} , and Zn^{2+}) involved in AD pathogenesis along with DNA protective potential against degenerative actions of $\cdot OH$ radicals. Molecular modelling studies confirm the potential of **13b** in blocking both PAS and CAS of AChE. In addition, interactions of **13b** with $A\beta_{1-42}$ monomer are also streamlined. Therefore, hybrid **13b** can act as an effective hit lead molecule for further development of selective AChE inhibitors as multifunctional anti-Alzheimer's agents.

Alzheimer's disease (AD) is the most prevalent (70–80% of all dementia forms) type of dementia in elderly people (usually 65 years and above) all around the globe characterized by progressive memory loss, impaired linguistic efficacy, mood disturbances, behavioural changes and cognitive impairments which finally carries toward death. It is a neurodegenerative disorder that starts slowly and gets worse over time with lost body functions that make the life of AD patient miserable and pose heavy monetary as well as a social burden to family and society.¹ Thus, it is a global emergency to control this disease without any delay.

Though the origin of AD is still ambiguous lifestyle, genetic and environmental factors are suggested to be involved in the onset as well as the progression of this disease.² Generation of toxic amyloid-beta ($A\beta$) protein and its extracellular plaques, as well as neurofibrillary tangles, originated from hyperphosphorylated tau proteins were considered as the two major pathological hallmarks of AD and no standard treatment was available for this disease until Davies and Maloney (in 1973) proposed cholinergic hypothesis.³ Following the same, four cholinesterases (acetylcholinesterase and butyrylcholinesterase)

inhibitors tacrine, donepezil, rivastigmine and galantamine were approved by the FDA. These drugs offer only palliative care and unable to freeze or reverse disease progression.⁴ One NMDA receptor antagonist (memantine) was also approved but it doesn't offer much relief similar to cholinesterase inhibitors.⁵ In last 20 years, apart from cholinergic, amyloid and tau protein cascade, various novel AD mechanisms have also been explored by the researchers that include inflammation, oxidative stress and deregulation of bio-metals, etc. suggesting multi-targeted nature of this disease.⁶ Along with the hydrolysis of acetylcholine (ACh), acetylcholinesterase enzyme (AChE) is found to promote $A\beta$ aggregation that interacts with its peripheral anionic site (PAS).⁷ Metal hemostasis in the brain of AD patient has been observed to be disturbed by extracellular elevation of zinc and copper along with the intracellular accumulation of iron. Copper and zinc were observed to bind with $A\beta$ and promote reactive oxygen species (ROS) by inducing its aggregation.⁸ Oxidative stress resulted from the abundance of redox-sensitive metals (Cu, Fe, and Zn) found to induce proteolysis of amyloid precursor protein via upregulating β -secretase that leads to an increase

* Corresponding authors.

E-mail addresses: singh.harbinder40@gmail.com (H. Singh), jatindervirsingh1@gmail.com (J. Vir Singh), bedi_preet@yahoo.com (P. Mohinder Singh Bedi).

<https://doi.org/10.1016/j.bmcl.2020.127477>

Received 12 May 2020; Received in revised form 1 August 2020; Accepted 5 August 2020

Available online 08 August 2020

0960-894X/ © 2020 Elsevier Ltd. All rights reserved.

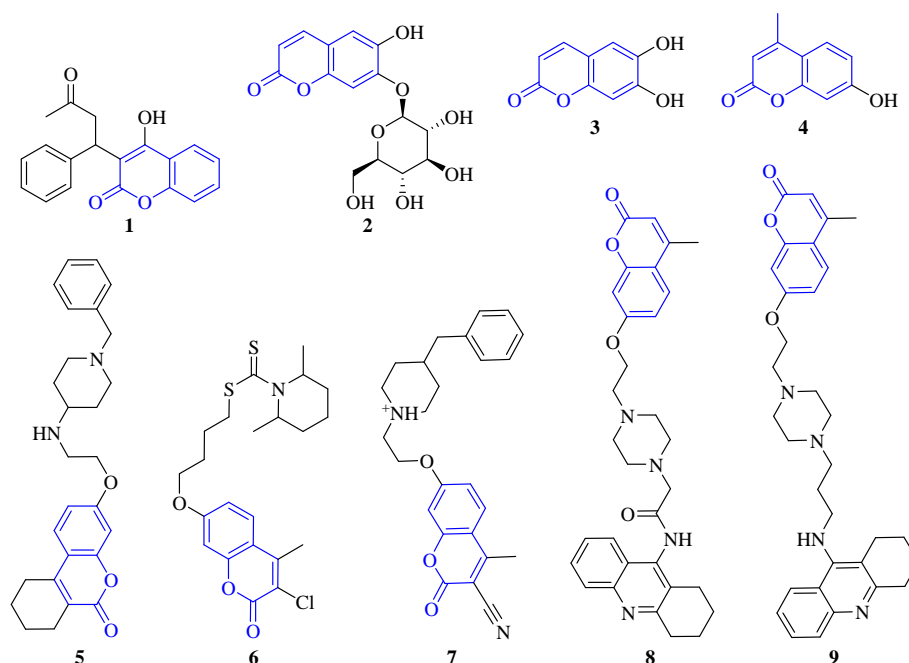


Fig. 1. Various coumarin derivatives in clinical practice (1–4) and multifunctional anti-Alzheimer's agents (5–9).

in A β . Iron was found to delay ordered aggregation of A β that promotes its toxicity. Chelation of iron was observed to provide protection from A β toxicity.⁹

Coumarins (benzopyran-2-ones) offer a potential class of compounds that possess a wide range of therapeutic properties (Fig. 1). Numerous coumarin derivatives like warfarin as an anticoagulant (1), esculin as vasoprotective (2), scopoletin as anti-inflammatory (3), hymecromone as an antispasmodic (4), etc. are already in clinical practice. Besides this, coumarin derivatives are reported to have a diverse range of biological activities like antioxidant, anticancer, antidepressant, antinociceptive, hepatoprotective, antibacterial, antifungal, antiviral, antidiabetic and anti-Alzheimer's. Especially in Alzheimer's drug development, multifunctional coumarin hybrids (5–9) have also been reported with promising results.¹⁰

Benzotriazole is a versatile nucleus in the field of medicinal chemistry and has long known metal chelating properties. In past two decades, a wide range of biologically active molecules has been designed by researchers across the globe in which benzotriazole is acting as a core nucleus itself or modulating the activity of other biologically active pharmacophores (Fig. 2). Benzotriazole derivatives designed so far has shown potential biological activities such as antibacterial (10), anti-tuberculosis (11), antifungal (12), antiviral (13), antiprotozoal (14), anticancer (15), antiemetic (16), antioxidant (17), and anti-inflammatory (18), etc.¹¹

Molecular hybridization is a well-established stratagem that involves combining two or more pharmacophores with or without any linker and provides a single hybrid molecule having properties of all combined bioactive substances. Molecular hybridization remains successful in giving various potential candidates to clinical trials within the last 30 years that includes MCB3837, Ro 23–9424, CBR-2092, and TD-1792 etc.^{12,13} Triazole is a well-known bioactive moiety that has been successfully utilized for the development of potential bioactive compounds (Fig. 3) including multifunctional anti-Alzheimer's agents (23–28).^{14–17} Molecular docking studies of these multifunctional agents suggest that triazole more fondly interacts with acetylcholine binding site of AChE and impart higher selectivity toward AChE over butyrylcholinesterase (BuChE).¹⁸ Triazole linker appropriately separating two active pharmacophores, was observed for introducing anti-A β aggregation properties in the molecule.¹⁹

Peripheral anionic site (PAS) of AChE interacts with A β fragment and promotes its aggregation while catalytic anionic site (CAS) selectively accepts ACh. Donepezil is the only drug that interacts simultaneously with both PAS and CAS of AChE enzyme, which may be the possible reason for its dual AChE as well as A β aggregation inhibitory potential. These properties makes donepezil, a perfect template for Alzheimer's drug development.²⁰ The favourable skeleton of donepezil and strong pharmacophoric features of coumarin and benzotriazole along with the successful history of molecular hybridization with triazole linker provides a solid base for utilizing all of them in designing novel multifunctional anti-Alzheimer agents (Fig. 4). Thus considering the pressing need of potential multifunctional agents for the management of AD, novel triazole linked coumarin-benzotriazole hybrids based on donepezil skeleton template has been designed by taking account of Lipinski rule of 5 and ADME properties (Supplementary Table S1 and S2), synthesized via click chemistry approach and evaluated for their anti-Alzheimer potential.

Designed hybrid molecules were synthesized via a series of chemical reactions (Scheme 1). Coumarins i.e. 4-OH coumarin (1) and 7-OH coumarin (4) were reacted with various dibromoalkanes in the presence of K₂CO₃ at 25 °C in DMF yielded alkylated coumarins (2a–e and 5a–e). Alkylated coumarins were further treated with NaN₃ at 25 °C in DMF to form *N*-azidoalkyl coumarins (3a–e and 6a–e). Simultaneously, OH-benzotriazole (7) was reacted with propargyl bromide in the presence of K₂CO₃ at 25 °C in DMF to get 1-(prop-2-yn-1-yloxy)-1H-benzotriazole (7a). Propargylation of 1H-benzotriazole (8) was done under similar conditions as used for OH-benzotriazole resulted in 1-(prop-2-yn-1-yl)-1H-benzotriazole (8a) with 61% yield and 2-(prop-2-yn-1-yl)-2H-benzotriazole (8b) with 18% yield. Compound PBB (8a) was characterized by the appearance of two doublets at 8.09–8.07 ppm and 7.73–7.71 ppm for two individual flagpole protons present on the 4th and 7th position of benzene ring (Scheme 1), while in PBC (8b), these flagpole protons are appeared as merged signals in a multiplet at 7.91–7.95 ppm as these protons bear in same electromagnetic environment (refer to ¹H NMR of 8b in Supplementary data). Obtained propargylated benzotriazoles were treated with prepared *N*-azidoalkyl coumarins in the presence of the catalytic amount of copper sulfate and reducing agent sodium ascorbate at 25 °C in DMF yielded various triazole linked coumarin-benzotriazole hybrids.²¹

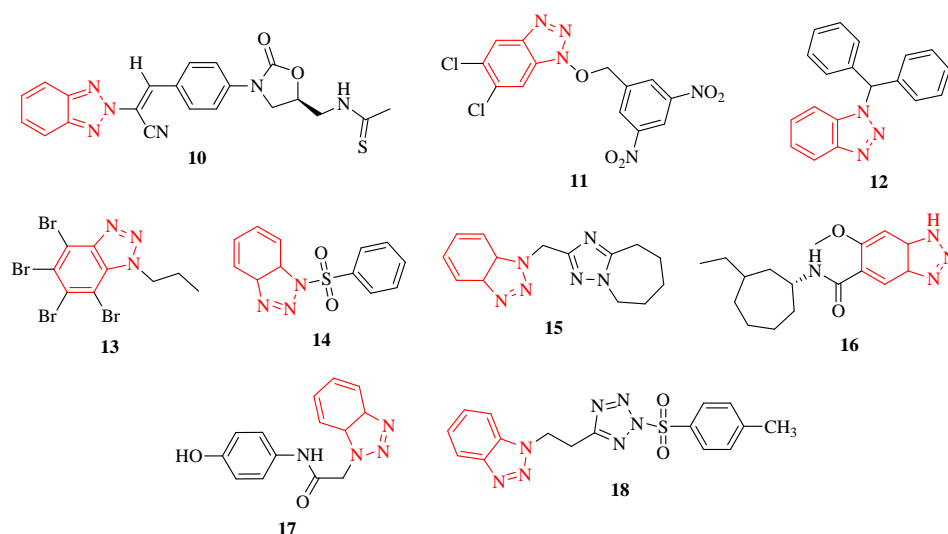


Fig. 2. Various biologically active benzotriazole derivatives (10–18).

As in the hydrolysis process of acetylcholine, 80% role is performed by AChE enzyme, while BuChE performs only a secondary role. Therefore, all the synthesized compounds were screened for their inhibitory potential against both AChE and BuChE enzymes using Ellman's method and compared with standard anticholinesterase drug donepezil. Data were obtained from triplicate experiments and presented as the mean \pm SD of three independent experiments (Table 1).

In the case of anti-AChE activity, compound **13b** emerged as the most potent one making 4-hydroxycoumarin linked with 1-benzotriazole via 1,2,3-triazole, the most suitable architect for AChE inhibition. Data from biological activity suggest that chain length of three carbons (**13b**) is most suitable for AChE inhibition and as the number of carbons between triazole and coumarin moiety increases, anti-AChE activity decreases accordingly (IC_{50} = 0.059 to 5.422 μ M from **13b** to **13e** respectively). A several-fold decrease in the anti-AChE activity was observed when 4-hydroxycoumarin was replaced with 7-hydroxycoumarin (as X) (compare **13b** with **10b**, **11b** with **14b**) suggesting that carbonyl group of 4-hydroxycoumarin lies toward triazole linker is suitable for anti-AChE activity as in donepezil (carbonyl group of indanone lies towards the piperidine moiety: Fig. 4). The chain length

between triazole (linker) and coumarin moieties greatly influence the inhibitory potential of the compounds. As the chain length increases, the inhibitory potential decreases. The chain length of three carbons was found most preferable for inhibitory activity. Most of the compounds with long-chain ($n > 4$) were found inactive against the enzyme (see **9d**, **9e**, and **10e**, **12c** to **12e**, **14d** and **14e**). 1-benzotriazole as Y and 4-hydroxycoumarin as X was found best combination that exhibited potent AChE inhibitory potential (**13a–13e**) amongst which compound **13b** was found to be endowed with most prominent AChE inhibition with the IC_{50} value of 0.059 μ M which is comparable to that of donepezil (IC_{50} = 0.039 μ M). While 1-hydroxy benzotriazole as Y and 7-hydroxycoumarin as X was an unsuitable combination for AChE inhibitory activity (**12a–12e**). Compounds consisting of 2-benzotriazole as Y and 4-hydroxycoumarin as X showed moderate inhibition of the enzyme (**11a–11e**). Therefore, overall preference of AChE inhibitory activity for coumarins is 4-hydroxycoumarin > 7-hydroxycoumarin, for benzotriazoles it is 1-benzotriazole > 2-benzotriazole > 1-hydroxy benzotriazole, and for carbon chain length it is 3 > 2 > 4 > 5 > 6. All the compounds were also evaluated for their inhibitory potential against butyrylcholinesterase (BuChE)

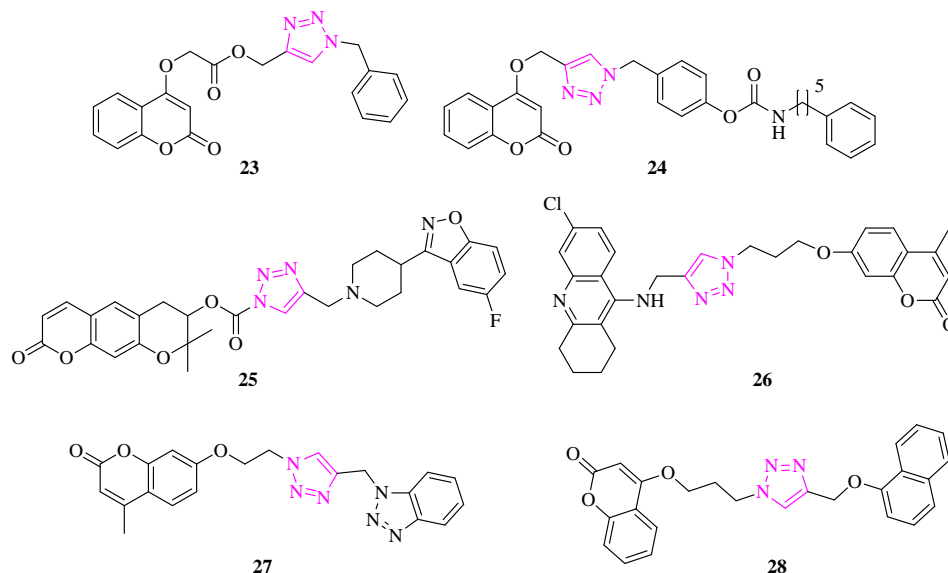


Fig. 3. Triazole linked hybrid molecules with anti-Alzheimer's activity (23–26).

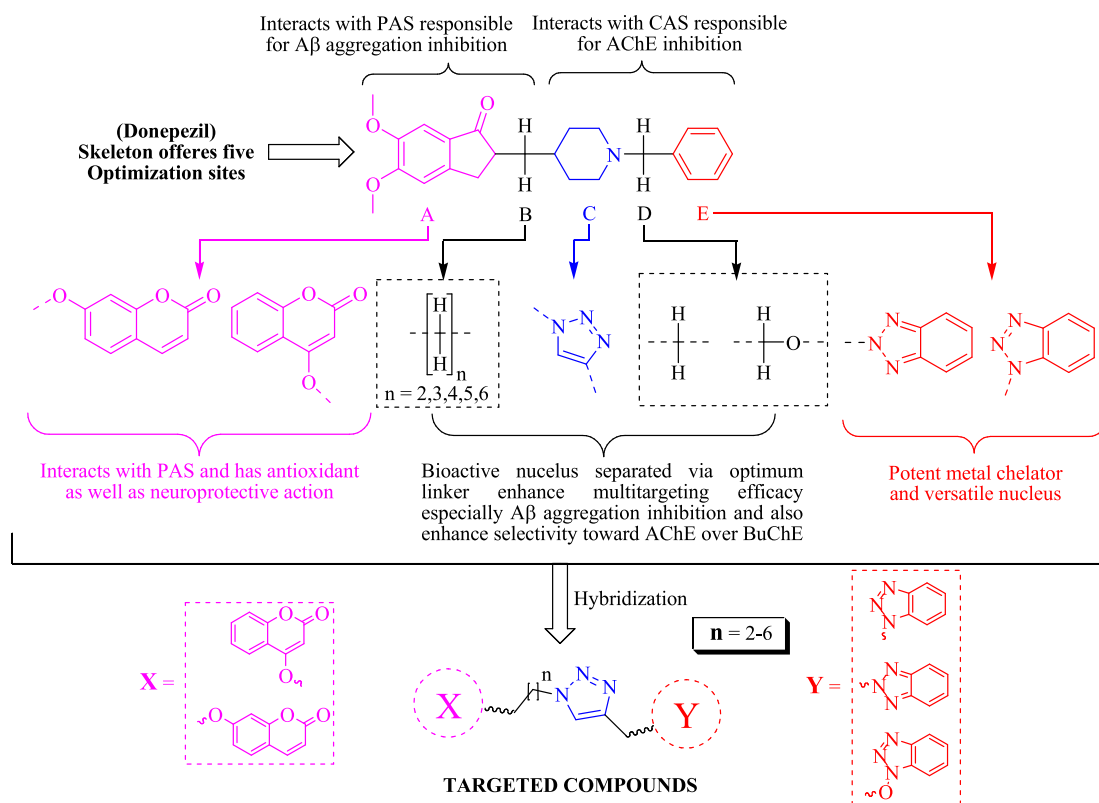


Fig. 4. Design strategy.

enzyme in a similar manner. None of the synthetic compounds showed inhibitory activity against the BuChE (IC_{50} above 10 μ M). The inhibitory potential of most potent AChE inhibitor **13e** was also tested at two more concentrations (at 50 & 100 μ M) against BuChE enzyme while no significant enhancement was observed in the inhibition against BuChE which suggests the significance of these hybrid compounds towards the selective inhibition of AChE enzyme. The compound showed most potent anti-AChE inhibition (**13b**) was further subjected to enzyme kinetic studies and reciprocal Lineweaver-Burk plot was plotted with three concentration levels. In reciprocal Lineweaver-Burk plot, increase in the slope (decreased V_{max}) as well as intercept (higher K_m) was observed with increasing concentrations of **13b** (Fig. 5). Intersection in 2nd quadrant of the reciprocal Lineweaver-Burk plot suggest that **13b** followed a mixed-type inhibitory pattern against AChE. The inhibition constant (K_i) for **13b** was calculated as 0.04167 nM.²²

Amyloid beta ($A\beta_{1-40}$ and $A\beta_{1-42}$) peptides originated from amyloid precursor protein plays an important role in the pathogenesis of Alzheimer's disease. $A\beta_{1-42}$ has higher pathogenicity as compare to $A\beta_{1-40}$ due to its higher tendency to form fibrillar aggregates that promote neuronal degeneration. In addition, Copper is well known to promote amyloid-beta aggregation in amyloid pathogenesis.²³ Thus, inhibition of $A\beta_{1-42}$ by an anti-Alzheimer's agent is a potential advantage. Considering this intention synthesized compounds were screened for their inhibitory action on copper-mediated $A\beta_{1-42}$ aggregation by employing Thioflavin T based fluorescence assay using curcumin as reference anti-amyloidogenic agent. At the concentration of 50 μ M, most of the compounds showed percentage inhibition below 10% except compounds bearing 1-benzotriazole moiety either it was attached with 4-hydroxycoumarin or with 7-hydroxycoumarin respectively. Percentage inhibition was up to 36.68% (Table 1) which was much lower as compare standard curcumin (62.26%). **13b** was able to inhibit $A\beta_{1-42}$ up to 34.26%.

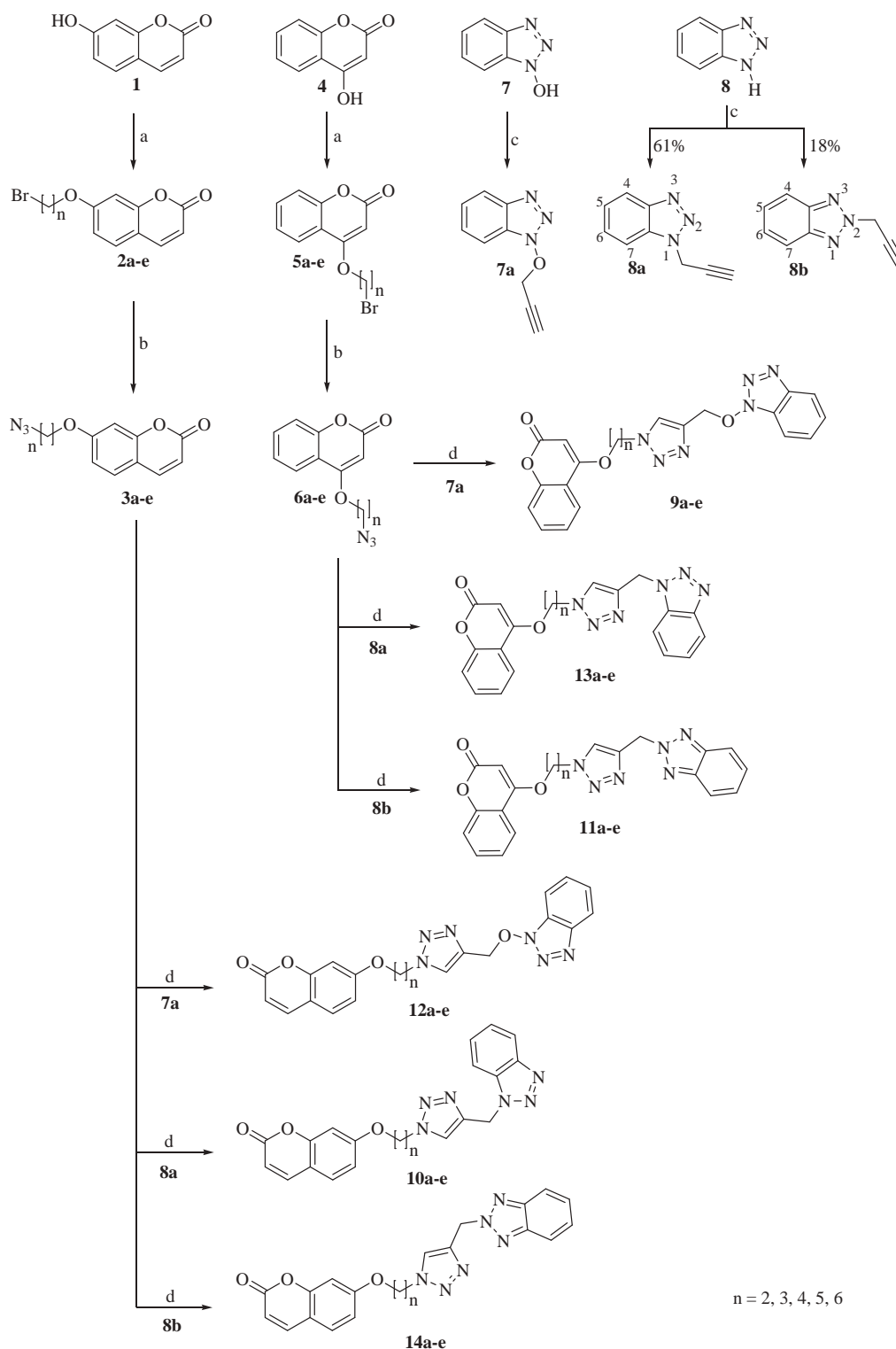
Amyloid plaques in AD brains are generally designated as 'metallic sinks' due to higher concentrations of Fe, Cu and Zn ions in them. These

metal ions trigger Fenton-type process and are attributed to higher oxidative stress in AD.²⁴ *In vitro* studies demonstrated the encouraging effect of these metals ions in A β toxicity through the generation of ROS in the presence of dioxygen.²⁵ Thus anti-Alzheimer's agents with metal chelating properties will be a significant advantage. UV-Vis spectra of **13b** showed an increase in absorption intensity and detectable blue shifts on the addition of Cu^{2+} , Fe^{2+} and Zn^{2+} while minor changes with Mg^{2+} were observed (Fig. 6A), proving the complex formation ability of **13b** with Cu^{2+} , Fe^{2+} and Zn^{2+} .²⁶ Stoichiometry of **13b**- Cu^{2+} complex was determined by employing a molar ratio method by titrating a solution of **13b** with gradually increasing amounts of $CuCl_2$. Absorption vs Cu^{2+} mole fraction plot (Supplementary Fig. S1: 6B) indicates the 2:1 stoichiometry of the **13b**- Cu^{2+} complex suggesting the possible efficacy of **13b** in the reduction of Cu^{2+} mediated A β aggregation and ROS generation.

Ageing and A β induced DNA damage have significant contribution to the progression of AD.²⁷ Increased DNA fragmentation and nicking have been detected in AD brains. Various ROS especially H_2O_2 mediated oxidative stress trigger DNA damage in AD.²⁸ Thus **13b** was further evaluated for its protective effect against Fenton-type oxidative cleavage of *pBR322* plasmid DNA. *pBR322* plasmid DNA exists in three major forms namely, supercoiled circular form (I), open circular (II), and linear form (III). In results, **13b** was able to prevent the conversion of the supercoiled circular form (I) of DNA to open circular (II) DNA and then linear form (III) DNA. Thus **13b** was able to protect DNA from degradative action of $\cdot OH$ radicals (Fig. 7).

Cell toxicity study was performed to evaluate the safety profile of **13b** on SH-SY5Y cells using donepezil as reference. After 24 h of incubation of **13b** or donepezil with SH-SY5Y cells, cell viability was evaluated using MTT assay. Both **13b** and donepezil showed negligible toxicity in concentrations ranging from 0.001 to 100 μ M, indicating the safety of **13b** in AD treatment (Fig. 8).

Molecular modelling studies were performed to get insight into various molecular interactions responsible for the modulation of



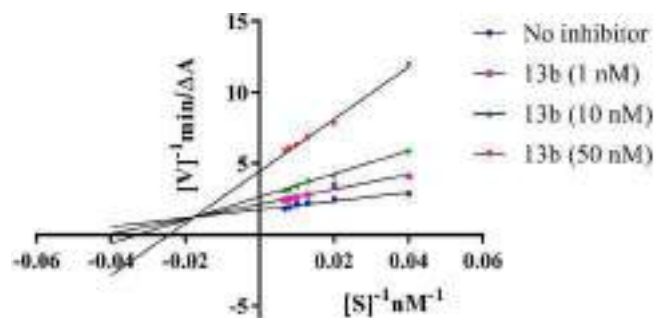
Scheme 1. Synthesis of triazole linked coumarin-benzotriazole hybrids. Reagents and conditions: (a) dibromoalkane, K_2CO_3 , DMF, 0.5 to 2 h, stir, rt; (b) NaN_3 , DMF, 1 to 2 h, stir, rt; (c) propargyl bromide, K_2CO_3 , DMF, 0.5 to 4 h, stir, rt; (d) sodium ascorbate, $CuSO_4$, DMF, 0.5 to 8 h, rt.

inhibitory activity of the most potent AChE inhibitor (**13b**). For that purpose, the X-ray crystallographic structure of recombinant human acetylcholinesterase complexed with donepezil (PDB entry: 4EY7; resolution, 2.3509 Å), was employed.²⁹ Accuracy of docking protocol was validated by docking co-crystallized ligand donepezil into its binding site. The program was capable to reproduce best fit confirmation of donepezil in chain B with root mean square deviation (RMSD) value of

0.965, indicating the reliability of docking protocol. After that **13b** was docked into donepezil binding site, and best pose with -18.5818 score having ΔG value of -38 kJ/mol was selected for discussion (Fig. 9). The overall binding mode of **13b** with residues of donepezil binding site suggest that compound is properly positioned in the cavity and well stabilized by various electrostatic interactions. Major interactions with AChE include van der Waals, π - σ , π - π stacked, π - π T-shaped and

Table 1AChE, BuChE and A β_{1-42} aggregation inhibition of synthesized compounds in comparison to Donepezil.

Comp.	X	Y	n	eeAChE ^b		A β_{1-42} aggregation inhibition (%) ^d
				IC ₅₀ (μ M) ^a	IC ₅₀ (μ M) ^a	
9a			2	4.322 \pm 0.056	≥ 10	16.22 \pm 1.28
9b			3	1.324 \pm 0.012	≥ 10	≤ 10
9c			4	3.233 \pm 0.027	≥ 10	≤ 10
9d			5	≥ 10	≥ 10	≤ 10
9e			6	≥ 10	≥ 10	≤ 10
10a			2	2.112 \pm 0.029	≥ 10	29.36 \pm 1.69
10b			3	2.924 \pm 0.016	≥ 10	15.86 \pm 1.48
10c			4	4.329 \pm 0.031	≥ 10	11.36 \pm 1.89
10d			5	5.429 \pm 0.038	≥ 10	≤ 10
10e			6	≥ 10	≥ 10	≤ 10
11a			2	1.890 \pm 0.023	≥ 10	≤ 10
11b			3	1.670 \pm 0.014	≥ 10	≤ 10
11c			4	2.093 \pm 0.016	≥ 10	≤ 10
11d			5	4.810 \pm 0.045	≥ 10	≤ 10
11e			6	6.233 \pm 0.019	≥ 10	≤ 10
12a			2	2.012 \pm 0.016	≥ 10	11.38 \pm 1.23
12b			3	1.978 \pm 0.026	≥ 10	≤ 10
12c			4	≥ 10	≥ 10	≤ 10
12d			5	≥ 10	≥ 10	≤ 10
12e			6	≥ 10	≥ 10	≤ 10
13a			2	0.097 \pm 0.045	≥ 10	36.68 \pm 2.17
13b			3	0.059 \pm 0.006	≥ 10	34.26 \pm 1.97
13c			4	0.234 \pm 0.061	≥ 10	22.36 \pm 1.81
13d			5	1.141 \pm 0.012	≥ 10	11.36 \pm 0.77
13e			6	5.422 \pm 0.032	≥ 10	≤ 10
14a			2	1.176 \pm 0.023	≥ 10	≤ 10
14b			3	1.156 \pm 0.013	≥ 10	≤ 10
14c			4	5.436 \pm 0.056	≥ 10	≤ 10
14d			5	≥ 10	≥ 10	≤ 10
14e			6	≥ 10	≥ 10	≤ 10
Donepezil				0.039 \pm 0.097	8.416 \pm 0.628	
Curcumin						62.26 \pm 2.92

^aIC₅₀: 50% inhibitory concentration (mean \pm SD of three individual experiments). ^bAChE obtained from electric eel. ^cBuChE obtained from equine serum.^dPercentage A β_{1-42} inhibition estimated by using Thioflavin T based fluorescence assay at a sample concentration of 50 μ M.**Fig. 5.** Overlaid Lineweaver-Burk plot derived from the kinetic study by using no and three concentrations of **13b** with varied substrate concentrations (0.025–0.0150 mM) depicting a mixed type of inhibition by compound **13b**.

conventional hydrogen bond interaction. The coumarin moiety has perfectly arranged itself in a cavity formed by two polar (Tyr72 and Tyr341) and two hydrophobic (Trp286 and Phe295) residues. The

backbone –NH of Phe295 make conventional hydrogen bond interaction with the carbonyl oxygen atom of coumarin (H-bond acceptor; $d = 2.802$ Å). Similar interaction of –NH in Phe295 backbone has been observed with ketonic oxygen of indanone moiety in donepezil but with little higher distance (H-bond acceptor; $d = 2.986$ Å) which highlight the stronghold of coumarin over indanone in the peripheral active site (PAS)

Both rings A and B of coumarin are showing π - π stacked interactions with indole ring in Trp286 backbone. Tyr72 and Tyr341 make van der Waals interactions with rings A and B of coumarin. OH on Tyr124 backbone also showing conventional hydrogen bond interaction (H-bond acceptor; $d = 2.042$ Å) with oxygen present between coumarin and three-carbon alkyl chain seems to promote the efficiency of **13b** for PAS. Triazole nucleus (Ring C) which acts as a linker between coumarin and benzotriazole makes π - π T-shaped interaction with hydroxyphenyl backbone of Tyr337 (π -Orbitals to π -Orbitals; $d = 5.634$ Å) whereas donepezil which makes π -Cation interaction with hydroxyphenyl backbone of Tyr337 with little shorter distance (π -Cation; $d = 4.665$ Å). Additional π - π T-shaped interaction of triazole nucleus

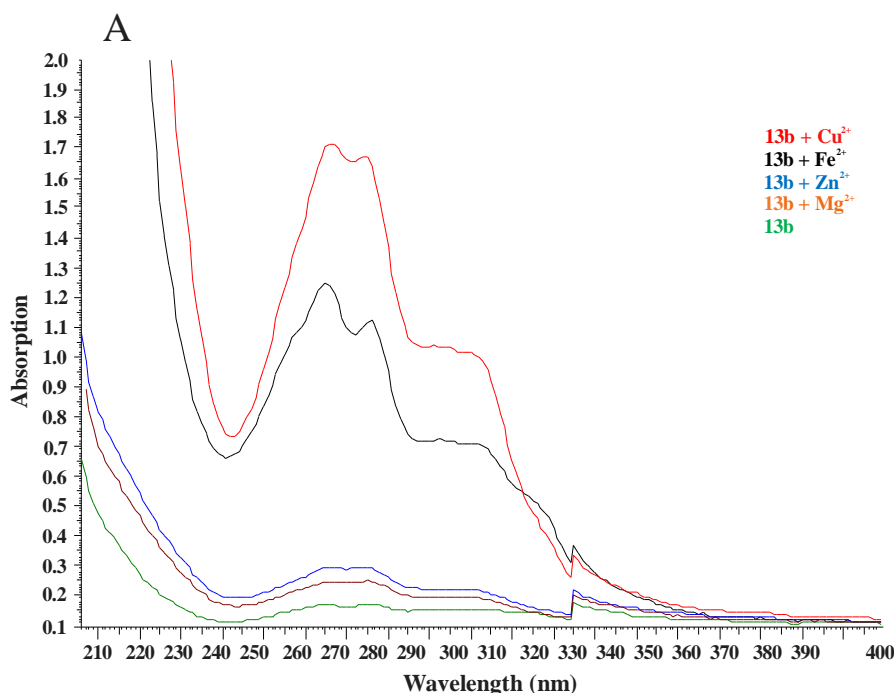


Fig. 6. A. Overlaid UV spectra of **13b** (5 μ M) itself alone and in the presence of Cu^{2+} , Fe^{2+} , Zn^{2+} , and Mg^{2+} (5 μ M).

has been observed with imidazole nucleus of His447 (π -Orbitals to π -Orbitals; $d = 5.349 \text{ \AA}$) which is absent on donepezil making triazole linker an interesting replacement of piperidine moiety in donepezil skeleton for AChE inhibition. The benzotriazole moiety is well-positioned in the cavity formed by five hydrophobic (Gly121, Trp86, Phe338, Phe297, and Gly120) and three polar residues (Ser125, Tyr124 and Tyr133). Nitrogen from ring D makes a conventional hydrogen bond with $-\text{OH}$ in Tyr133 backbone. Indole nucleus in Trp86 backbone makes similar but little closer crisscross type π - π stacked interaction (To ring D; π -Orbitals to π -Orbitals; $d = 4.435 \text{ \AA}$) with benzotriazole nucleus as the donepezil makes with its phenyl (To ring D; π -Orbitals; $d = 5.051 \text{ \AA}$). Additional π - σ interaction ($-\text{CH}_2-$ to π -Orbital; $d = 5.349 \text{ \AA}$) of ring E form benzotriazole with $-\text{CH}_2-$ of Trp86 backbone has been observed which was absent in donepezil to Trp86. Apart from this, Gly121, Ser125, Phe338, Phe297, Gly120 capture benzotriazole moiety through van der Waals interactions. The overall study

suggests that **13b** is well decorated with small, rigid and planar groups making the finest scaffold which is able to satisfy the necessary pharmacophoric requirements for AChE inhibition.

$\text{A}\beta_{1-42}$ aggregation inhibition and good interaction of **13b** toward PAS observed during docking in donepezil binding site of AChE further encourage us to study the interaction of **13b** with $\text{A}\beta_{1-42}$ monomer. For that purpose, the NMR elucidated structure of amyloid-beta ($\text{A}\beta_{1-42}$) monomer (PDB entry: 1IYT) was employed.³⁰ Sphere module of LeadIT was employed for defining binding site using a radius of 6.50 \AA . Previously prepared structure of **13b** was allowed to dock in prepared monomer amino acids. Best pose with -6.7274 was selected for discussion (Fig. 10).

The coumarin moiety of **13b** positioned itself in the cavity formed by two polar (Gln15 and Lys16) and one hydrophobic residue (Phe19). Gln15 shows conventional hydrogen bond interaction (H-bond acceptor; $d = 1.633 \text{ \AA}$) with oxygen ($-\text{O}-$) present in the ring B of

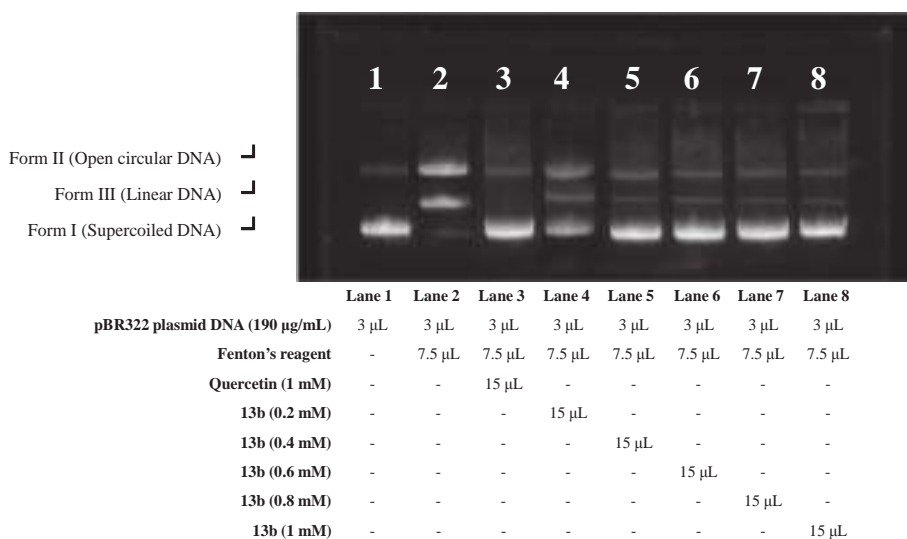


Fig. 7. DNA protection properties of **13b**; In lane 4 to 8 showing the capability of **13b** in preventing both open circular and linear cuts.

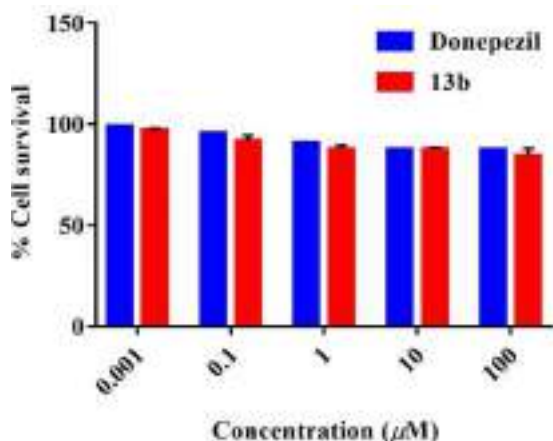


Fig. 8. Cytotoxicity study of **13b** in comparison with donepezil on SH-SY5Y cells. SH-SY5Y cells were incubated for 24 h with increasing concentrations of both **13b** and donepezil ranging from 0.001 to 100 μ M. Results are displayed as the percentage of viable cells with respect to untreated control cells. Values are expressed as the mean \pm SD obtained from three individual experiments.

coumarin through $-\text{NH}_2$ of its backbone. Another conventional hydrogen bond interaction (H-bond acceptor; $d = 1.896 \text{ \AA}$) is shown by a carbonyl oxygen atom of coumarin with core amino group of Lys16. These hydrogen bonds with very short distances showing the affinity of **13b** toward $\text{A}\beta_{1-42}$. Phenyl ring of Phe20 backbone showing π - π stacked interactions with both ring A and B of coumarin. Free nitrogen atoms of triazole moiety also showed conventional hydrogen bond interaction (H-bond acceptor; $d = 2.376 \text{ \AA}$) with Lys16 through amine group in its backbone. Carbon hydrogen bond interaction is also observed between Val12 and the carbonyl oxygen atom of coumarin through the core hydrogen of Val12. Nitrogen in ring D of benzotriazole

makes π -lone pair interaction (lone pair to π -Orbital; $d = 2.912 \text{ \AA}$) with Phe20 through the phenyl group in its backbone. Asp23 showing van der Waals interactions with both coumarin and benzotriazole moieties via Phe19 (H-bond acceptor; $d = 1.833 \text{ \AA}$) and Phe20 (H-bond acceptor; $d = 2.662 \text{ \AA}$) by making conventional hydrogen bond interactions with them. $\text{A}\beta_{1-42}$ are susceptible to form β -pleated “hairpin” like architects that are aggregated into fibrous form, and stabilized by hydrophobic interactions and salt bridge due to interactions between Asp23 and Lys28 residues in them. Docking study suggests the possible interaction of **13b** with Asp 23 of $\text{A}\beta_{1-42}$ monomer while strong and short distance interactions with other residues can certainly change the conformation of $\text{A}\beta_{1-42}$ monomer.

In summary, this study involved the rational design of triazole tethered coumarin-benzotriazole hybrid molecules based on donepezil skeleton, their synthesis, and evaluation as multifunctional agents against AD. Compounds were synthesized using click chemistry approach and characterized by ^1H , ^{13}C NMR and elemental analysis. Among all synthesized compounds **13b** emerged as the most potent *ee*AChE inhibitor with mixed type of inhibitory pattern. Structure-activity relationship revealed that distance of three-carbon alkyl chain between coumarin and triazole linker is well tolerable for AChE inhibition. The combination of 4-hydroxycoumarin and 1-benzotriazole linked through triazole with three carbon chains was found the most suitable combination for AChE inhibition. The insensitivity of these hybrids towards BuChE inhibition suggesting that the compounds are selective AChE inhibitors. **13b** inhibit copper-induced $\text{A}\beta_{1-42}$ aggregation and have chelating properties for metal ions (Cu^{2+} , Fe^{2+} , and Zn^{2+}) involved in AD pathogenesis. DNA nicking assay confirms the ability of **13b** to protect DNA from degenerative actions of $\cdot\text{OH}$ radicals. Various binding interactions with hAChE justify the potential of **13b** in blocking both PAS and CAS. Interactions of **13b** with $\text{A}\beta_{1-42}$ monomer are also streamlined. Besides having such potential multifunctional actions, coumarin and benzotriazole in **13b** provide

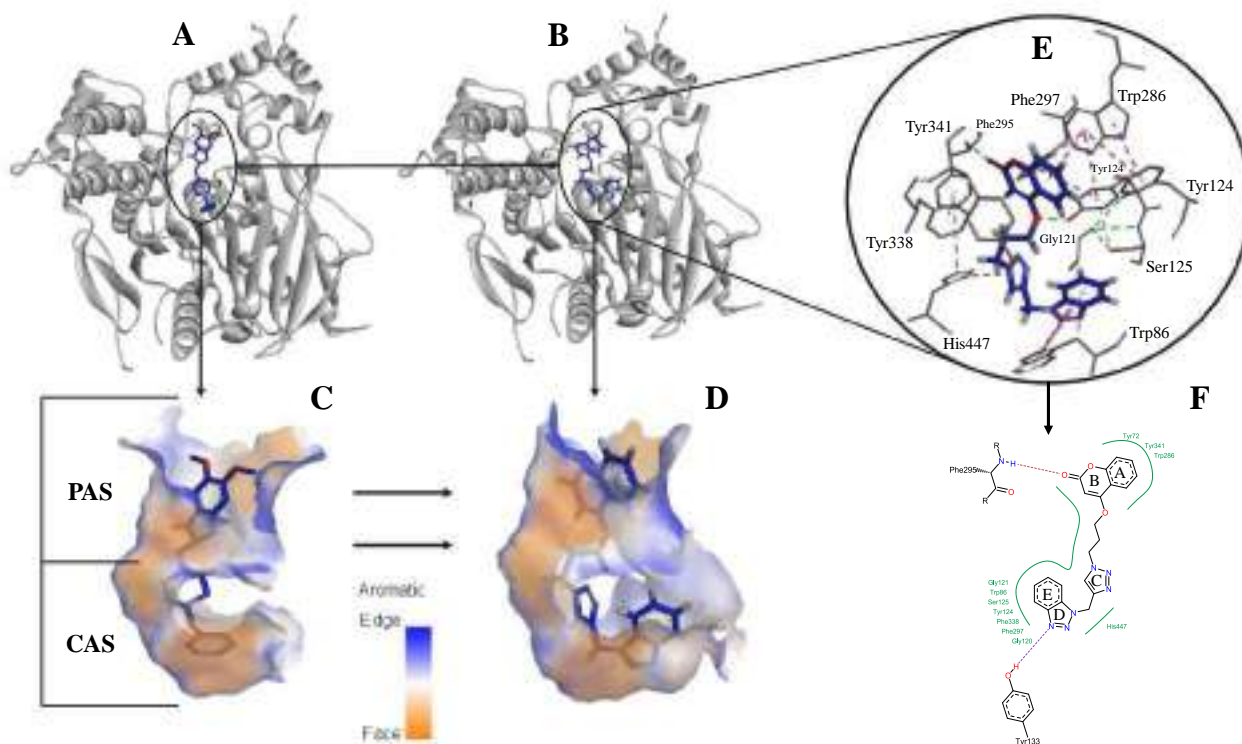


Fig. 9. (A) Acetylcholinesterase (AChE) enzyme complexed with donepezil (PDB entry: 4EY7; Resolution: 2.3509 \AA); (B) **13b** docked on the binding site of donepezil; (C) Donepezil positioned in the pocket made by active site residues shown using aromatic surface interactions; (D) **13b** positioned in the pocket made by active site residues shown using aromatic surface interactions; (E) 3D view of interactions of **13b** with residues of donepezil binding site in AChE; (F) 2D view of interactions of **13b** with residues of donepezil binding site in AChE.

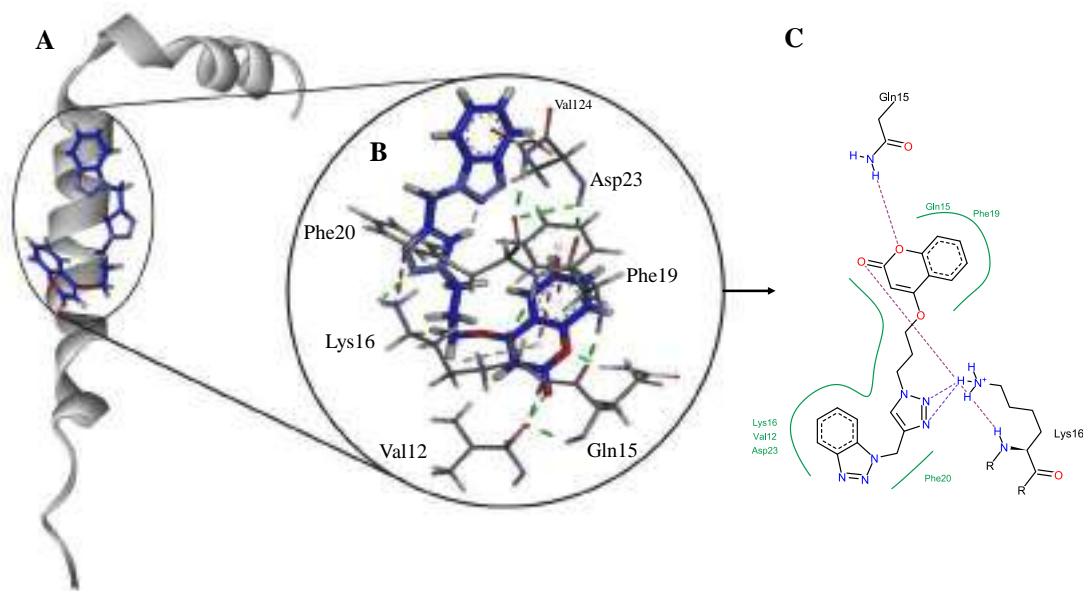


Fig. 10. (A) Amyloid beta ($A\beta_{1-42}$) monomer (PDB entry: 1IYT) complexed with **13b**; (B) 3D view of interactions of **13b** with residues of $A\beta_{1-42}$; (f) 2D view of interactions of **13b** with residues of $A\beta_{1-42}$.

considerable space for further improving the biological potential of the molecule and thus providing a hit lead for further development of safer and potent selective AChE inhibitors as multifunctional anti-Alzheimer's agents.

Declaration of Competing Interest

The authors declare that they have no known competing financial interests or personal relationships that could have appeared to influence the work reported in this paper.

Acknowledgements

Authors are grateful to the University Grants Commission for providing funds under National Fellowship for Other Backward Classes (NFOBC) to AS, Rajiv Gandhi National Fellowship (RGNF) to HS, Council of Scientific and Industrial Research (CSIR: 02(0319)17/EMR-II) to JVS, Department of Science and Technology for DST-Purse to HKG, WOS-A to KB and DST-FIST. The authors are also thankful to Guru Nanak Dev University, Amritsar for providing various facilities to carry out the research work.

Appendix A. Supplementary data

Supplementary data to this article can be found online at <https://doi.org/10.1016/j.bmcl.2020.127477>.

References

- (a) Finder VH. Alzheimer's disease: a general introduction and pathomechanism. *J. Alzheimer's Dis.* 2010;22:5-9; (b) <https://www.who.int/news-room/fact-sheets/detail/dementia>; 2020 Accessed 20 January 2020.
- Oakley H, Cole SL, Logan SE, Maus E, Shao P, Craft J, Guillozet-Bongaerts A, Ohno M, Disterhoft J, Eldik LV, Berry R, Vassar R. Intraneuronal β -Amyloid aggregates, neurodegeneration and neuron loss in transgenic mice with five familial Alzheimer's disease mutations: Potential factors in amyloid plaque formation. *J. Neurosci.* 2006;26:10129-10140.
- Davies P, Maloney AJF. Selective loss of central cholinergic neurons in Alzheimer's disease. *Lancet.* 1976;308:1403.
- (a) Romero A, Cacabelos R, Oset-Gasque MJ, Samadi A, Marco-Contelles J. Novel tacrine-related drugs as potential candidates for the treatment of Alzheimer's disease. *Bioorg Med Chem Lett.* 2013;23:1916-1922;
- (b) Rogers SL, Doody RS, Mohs RC, Freidhoff LT. Donepezil improves cognition and global function in Alzheimer's disease: a 15-week, double-blind, placebo-controlled study. Donepezil study group. *Arch Intern Med.* 1998;158:1021-1031;
- (c) Raskind MA, Peskind ER, Wessel T, Yuan W. Galantamine in AD: A 6-month randomized, placebo-controlled trial with a 6-month extension. The galantamine USA-1 study group. *Neurology.* 2000;54:2261-2268;
- (d) Saeedi M, Safavi M, Karimpour-Razkenari E, et al. Synthesis of novel chromones linked to 1,2,3-triazole ring system: Investigation of biological activities against Alzheimer's disease. *Bioorg Chem.* 2017;70:86-93.
- Marum RJV. Update on the use of memantine in Alzheimer's disease. *Neuropsych Dis Treat.* 2009;5:267-247.
- (a) Erlanson DA, Fesik SW, Hubbard RE, Jahnke W, Jhoti H. Twenty years on: the impact of fragments on drug discovery. *Nat. Rev. Drug Discov.* 2016;15:605-619; (b) Butterfield DA, Swomley AM, Sultana R. Amyloid β -peptide (1-42) induced oxidative stress in Alzheimer's disease: Importance in disease pathogenesis and progression. *Antioxid. Redox Signal.* 2013;19:823-835; (c) Tuppo EE, Arias HR. The role of inflammation in Alzheimer's disease. *Int. J. Biochem. Cell Biol.* 2005;37:289-305; (d) <https://www.medpagetoday.com/neurology/alzheimersdisease/75075>; 2020 Accessed 18 January 2020; (e) <https://sciencenordic.com/alzheimers-disease-denmark-forskerzonen/no-new-drugs-for-alzheimers-disease-in-15-years/1454636>; 2020 Accessed 18 January 2020.
- Alvarez A, Opazo C, Alarcon R, Garrido J, Inestrosa NC. Acetylcholinesterase promotes the aggregation of amyloid-beta-peptide fragments by forming a complex with the growing fibrils. *J. Mol. Biol.* 1997;272:348-361; (b) Vafadarnejad F, Mahdavi M, Karimpour-Razkenari E, Edraki N, Sameem B, Khanavi M, Saeedi M, Akbarzadeh T. Design and synthesis of novel coumarin-pyridinium hybrids: In vitro cholinesterase inhibitory activity. *Bioorg. Chem.* 2018;77:311-319.
- Greenough MA, Camakaris J, Bush AI. Metal dyshomeostasis and oxidative stress in Alzheimer's disease. *Neurochem Int.* 2013;62:540-555.
- (a) Bush AI. The metal theory of Alzheimer's disease. *J Alzheimer's Dis.* 2015;33:S277-S281;
- (b) Robert A, Liu Y, Nguyen M, Meunier B. Regulation of copper and iron homeostasis by metal chelators: a possible chemotherapy for Alzheimer's disease. *Acc Chem res.* 2015;48:1332-1339;
- (c) Watt NT, Whitehouse LJ, Hopper NJ. The role of zinc in Alzheimer's disease. *Int J Alzheimer's Dis.* 2011;971021.
- (a) He Q, Liu J, Lan JS, et al. Coumarin-dithiocarbamate hybrids as novel multi-target AChE and MAO-B inhibitors against Alzheimer's disease: design, synthesis and biological evaluation. *Bioorg Chem.* 2018;81:512-528;
- (b) Xie SS, Wang X, Jiang N, et al. Multi-target tacrin-coumarin hybrids: Cholinesterase and monoamine oxidase B inhibition properties against Alzheimer's disease. *Eur J Med Chem.* 2015;95:153-165;
- (c) Singh A, Singh JV, Rana A, et al. Monocarbonyl curcumin-based molecular hybrids as potent antibacterial agents. *ACS Omega.* 2019;4:11673-11684;
- (d) Bhagat K, Bhagat J, Gupta MK, et al. Design, synthesis, antimicrobial evaluation, and molecular modeling studies of novel indolinedione-coumarin molecular hybrids.

- ACS Omega. 2019;4:8720–8730;
- (e) Singh H, Singh JV, Bhagat K, et al. Rational approaches, design strategies, structure activity relationship and mechanistic insights for therapeutic coumarin hybrids. *Bioorg Med Chem*. 2019;27:3477–3510.
11. (a) Abudalo RA, Abudalo MA, Hernandez MT. Stability of benzotriazole derivatives with free Cu, Zn, Co and metal-containing enzymes: binding and interaction of methyl-benzotriazoles with superoxide dismutase and vitamin B12. *IOP Conf Ser Mater Sci Eng*. 2018;305:012024;
 - (b) Das J, Rao CVL, Sastry TVRS, et al. Effects of positional and geometrical isomerism on the biological activity of some novel oxazolidinones. *Bioorg Med Chem Lett*. 2005;2005(15):337–343;
 - (c) Augustynowicz-Kopec E, Zwolska Z, Orzesko A, Kazimierczuk Z. Synthesis and antimycobacterial activity of selected nitrobenzoxylated benzotriazoles. *Acta Pol Pharm*. 2008;65:435–439;
 - (d) Rezaei Z, Khabnadideh S, Zomorodian K, et al. Design, synthesis and antifungal activity of some new imidazole and triazole derivatives. *Arch Pharm Chem Life Sci*. 2011;344:658–665;
 - (e) Bretner M, Baier A, Kopanska K, et al. Synthesis and biological activity of 1H-benzotriazole and 1H-benzimidazole analogues—inhibitors of the NTPase/helicase of HCV and of some related Flaviviridae. *Antiviral Chem Chemother*. 2005;16:315–326;
 - (f) Al-Soud YA, Al-Masoudi NA, Ferwanah AES. Synthesis and properties of new substituted 1,2,4-triazoles: potential antitumor agents. *Bioorg Med Chem*. 2003;11:1701–1708;
 - (g) Rajasekaran A, Rajagopal KA. Synthesis of some novel triazole derivatives as anti-nociceptive and anti-inflammatory agents. *Acta Pharm*. 2009;59:355–364;
 - (h) Caliendo G, Carlo RD, Meli R, et al. Synthesis and trazodone-like pharmacological profile of 1- and 2-[3-[4-(X)-1-piperazinyl]-propyl]-benzotriazoles. *Eur J Med Chem*. 1993;28:969–1674;
 - (i) Briguglio I, Piras S, Corona P, Gavini E, Nieddu M, Carta BA. Benzotriazole: An overview on its versatile biological behavior. *Eur J Med Chem*. 2015;97:612–648.
12. Viegas-Junior C, Danuello A, Bolzani VDS, Barreiro EJ, Fraga CAM. Molecular hybridization: A useful tool in the design of new drug prototypes. *Curr Med Chem*. 2007;14:1829–1852.
 13. (a) Xu JH, Fan YL, Zhou J. Quinoline-triazole hybrids and their biological activities. *J Heterocyclic Chem*. 2018;55:1854–1862;
 - (b) Domaloan R, Idowu T, Zhanel GG, Schweizer F. Antibiotic hybrids: The next generation of agents and adjuvants against Gram-negative pathogens? *Clin Microbial Rev*. 2018;31:e00077–e117.
 14. Fan YL, Ke X, Liu M. Coumarin-triazole hybrids and their biological activities. *J Heterocyclic Chem*. 2018;5:791–802.
 15. (a) Dong H, Yuede CM, Coughlan CA, Murphy KM, Csernansky JG. Effects of donepezil on amyloid- β and synapse density in the Tg2576 mouse model in Alzheimer's disease. *Brain Res*. 2009;1303:169–178;
 - (b) Junaid M, Islam N, Hossain MK, Ullah MO. Metal based donepezil analogues designed to inhibit human acetylcholinesterase for Alzheimer's disease. *PLoS ONE*. 2019;14:e0211935.
 16. Torres FC, Goncalves GA, Vanzolini KL, et al. Combining the pharmacophore features of coumarins and 1,4-substituted 1,2,3-triazoles to design new acetylcholinesterase inhibitors: Fast and easy generation of 4-methylcoumarins/1,2,3-triazoles conjugates via click chemistry. *J Braz Chem Soc*. 2016;27:1541–1550.
 17. Mamgain R. Cu(I) catalyzed coumarin-1,2,3-triazole hybrids: Click chemistry. *Asian J Chem*. 2019;31:2543–2547.
 18. Riaz N, Iftikhar M, Saleem M, et al. New synthetic 1,2,4-triazole derivatives: Cholinesterase inhibition and molecular docking studies. *Results Chem*. 2020;2:100041.
 19. Jalili-Baleh L, Forootanfar H, Kucukkilinc TT, et al. Design, synthesis and evaluation of novel multi-target-directed ligands for treatment of Alzheimer's disease based on coumarin and lipoic acid scaffolds. *Eur J Med Chem*. 2018;152:600–614.
 20. Sameen B, Saeedi M, Mahdavi M, et al. Synthesis, docking study and neuroprotective effects of some novel pyrano[3,2-c]chromene derivatives bearing morpholine/phenylpiperazine moiety. *Bioorg Med Chem*. 2017;25:3980–3988.
 21. A catalytic amount of copper sulphate and sodium ascorbate was added to a solution of propargylated benzotriazoles (1 equiv) and azidated coumarins (1 equiv). The reaction mixture was allowed to stir at room temperature until it was completed (monitored by TLC). After completion, the reaction mixture was poured on crushed ice to eliminate copper sulfate and sodium ascorbate, set aside for some time (until ice converted into the water completely), filtered and dried to get the crude product. Obtained crude product was purified by using column chromatography using hexane: ethyl acetate (6: 4) to get triazole tethered coumarin benzotriazole hybrids. All the hybrids were synthesized in similar manner. Characterization data of most potent compound 4-(3-(4-((1H-benzo[d][1,2,3]triazol-1-yl)methyl)-1H-1,2,3-triazol-1-yl)propoxy)-2H-chromen-2-one (13b). Yield 74%, mp 166–168° C. Yellowish powder. ¹H NMR (500 MHz, DMSO-d₆) δ 8.32 (s, 1H), 8.04–8.03 (m, 1H), 7.90–7.88 (d, J = 10 Hz, 1H), 7.74–7.72 (d, J = 10 Hz, 1H), 7.66–7.63 (m, 1H), 7.55–7.52 (m, 1H), 7.41–7.38 (m, 2H), 7.34–7.31 (m, 1H), 6.04 (s, 2H), 5.85 (s, 1H), 4.61–4.58 (m, 2H), 4.22–4.19 (m, 2H), 4.39–4.37 (m, 2H). ¹³C NMR (125 MHz, DMSO-d₆) δ 165.19, 162.78, 162.04, 153.18, 146.02, 142.13, 133.21, 127.84, 124.87, 124.54, 123.45, 119.60, 116.84, 115.54, 111.32, 91.07, 67.12, 47.21, 43.41, 36.24, 29.13. Anal. Calcd for C₂₁H₁₈N₆O₃: C, 62.68; H, 4.51; N, 20.88. Found: C, 62.63; H, 4.45; N, 20.81.
 22. Sonmez F, Kurt BZ, Gazioglu I, et al. Design, synthesis and docking study of novel coumarin ligands as potential selective acetylcholinesterase inhibitors. *J Enzyme Inhib Med Chem*. 2017;32:285–297.
 23. Butterfield DA, Swomley AM, Sultana R. Amyloid β -peptide (1–42) induced oxidative stress in Alzheimer's disease: importance in disease pathogenesis and progression. *Antioxid Redox Signal*. 2013;19:823–835.
 24. Maynard CJ, Bush A, Masters C, Cappai R, Li QX. Metals and amyloid- β in Alzheimer's disease. *Int. J. Exp. Pathol*. 2005;86:147–159; (b) V.B. Kenche, K.J. Barnaham. Alzheimer's disease & metals: therapeutic opportunities. *Br. J. Pharmacol*. 2011;163:211–219.
 25. Cheignon C, Tomas M, Dt Bonnefont-Rousselot, Faller P, Hureau C, Collin F. Oxidative stress and the amyloid beta peptide in Alzheimer's disease. *Redox Biol*. 2018;14:450–464.
 26. Friggeri L, Vita DD, Pandolfi F, et al. Design, synthesis and evaluation of 3,4-dihydroxybenzoic acid derivatives as antioxidants, bio-metal chelating agents and acetylcholinesterase inhibitors. *J Enzyme Inhib Med Chem*. 2015;30:166–172.
 27. Mao P, Reddy PH. Aging and amyloid beta-induced oxidative DNA damage and mitochondrial dysfunction in Alzheimer's disease: Implications for early intervention and therapeutics. *Biochim Biophys Acta*. 2011;1812:1359–1370.
 28. (a) Reddy VP, Perry G, Cooke MS, Sayre LM, Smith MA. Mechanisms of DNA damage and repair in Alzheimer's disease. *DNA repair and human disease*. Boston, MA: Medical Intelligence Unit. Springer; 2006:98–113;
 - (b) Monte SMDL, Luong T, Neely TR, Robinson D, Wands JR. Mitochondrial DNA damage as a mechanism of cell loss in Alzheimer's disease. *Lab Invest*. 2000;80:1323–1335.
 29. Cheung J, Rudolph MJ, Burshteyn F, Cassidy MS, Gary EN, Love J, Franklin MC, Height JJ. Structures of human acetylcholinesterase in complex with pharmacologically important ligands. *J. Med. Chem*. 2012;55:10282–10286; (b) <https://www.rcsb.org/structure/4EY7> (Retrieved on 2/09/2019).
 30. Crescenzi O, Tomaselli S, Guerrini R, Salvadori S, D'Ursi AM, Temussi PA, Picone D. Solution structure of the Alzheimer amyloid beta-peptide (1–42) in an a polar microenvironment. Similarity with a virus fusion domain. *Eur. J Biochem*. 2002;269:5642–5648; (b) <https://www.rcsb.org/structure/1iyt> (Retrieved on 2/09/2019).